DILUTED HALIDE BASED IONIC LIQUIDS FOR WIDEN POTENTIAL WINDOW TO ENHANCE THE EDL-BASED SUPERCAPACITOR PERFORMANCE

by

Ragib Shakil

A THESIS SUBMITTED IN PARTIAL FULFILLMENT OF THE REQUIREMENT FOR THE DEGREE

OF

MASTER OF SCIENCE IN CHEMISTRY

Department of Chemistry

BANGLADESH UNIVERSITY OF ENGINEERING AND TECHNOLOGY (BUET), DHAKA-1000

April 2022

CANDIDATE'S DECLARATION

It is hereby declared that this thesis or any part of it has not been submitted elsewhere for the award of any degree or diploma.

…….……

(Ragib Shakil)

Signature &Name of the Candidate

Bangladesh University of Engineering and Technology (BUET), Dhaka-1000
Department of Chemistry

Certification of Thesis

A thesis on

DILUTED HALIDE BASED IONIC LIQUIDS FOR WIDEN POTENTIAL WINDOW TO ENHANCE THE EDL-BASED SUPERCAPACITOR PERFORMANCE

by

Ragib Shakil

Roll No.: 0419032704F, Session: April-2019, has been accepted as satisfactory in partial fulfilment of the requirements for the degree of Master of Science (M.Sc.) in Chemistry and certify that the student has demonstrated satisfactory knowledge of the field covered by this thesis in an oral examination held on April 27, 2022

Board of Examiners

1. Dr. Al-Nakib Chowdhury
Professor
Department of Chemistry
BUET, Dhaka-1000.

Supervisor & Chairman

2. Dr. Md. Abdur Rashid
Professor and Head
Department of Chemistry
BUET, Dhaka-1000

Member (Ex-officio)

2. Dr. Md. Shakhawat Hossain Firoz
Professor
Department of Chemistry
BUET, Dhaka-1000

Member

4. Dr. Chanchal Kumar Roy
Assistant Professor
Department of Chemistry
BUET, Dhaka-1000

Member

5. Dr. Md. Mominul Islam
Professor
Department of Chemistry
University of Dhaka, Dhaka -1000

Member (External)

DEDICATED TO

Kazi Rifat Mamun

I dedicate this thesis to my beloved friend late Kazi Rifat Mamun (1995-2019).

Kazi Rifat Mamun was an M.Sc student of the Department of Chemistry, BUET (April-2019) session. In late 2019, Rifat died of Guillain-Barré syndrome (GBS).

He had completed his B.Sc degree in Chemistry from Khulna University in 2019. Rifat was a talented young star and dedicated person who involved himself in fundamental research. He was a very brilliant, polite, innocent person I have ever seen. May Allah grant his soul and award him Jannah.

He came along with Me, and Mahamudul Hasan Rumon to get himself enrolled in the M.Sc program. They were passing their life with tremendous joy and happiness. It is suspected that Rifat got ill after consuming contaminated water or food. But, in reality, the exact reason for GBS is yet unknown

Table of Contents

List of Figures

List of Scheme

List of Tables

List of Abbreviations

EDLC – Electric Double Layer Capacitor

SC – Supercapacitor

IL – Ionic Liquid

OE – Organic Liquid

OVW – Operating Voltage Window

NMP – *N*-Methyl-2-pyrrolidone

PVDF – Polyvinylidene difluoride

GO – Graphene Oxide

rGO – Reduced Graphene Oxide

C_{sp} – Specific Capacitance

E – Energy Density

P – Power Density

R_s – Solution Resistance

CV – Cyclic Voltammetry

GCD – Galvanostatic Charging-Discharging

EIS – Electrochemical Impedance Spectroscopy

Acknowledgment

At the very beginning, I humbly acknowledge my deepest gratitude to the almighty, the most gracious, benevolent, and merciful creator for his infinite mercy bestowed on me in carrying out the research work presented in the dissertation.

It is a great pleasure for me to acknowledge my deepest sense of gratitude, sincere appreciation, heartfelt indebtedness, and solemn regards to my reverend teacher and supervisor Dr. Al-Nakib Chowdhury, Professor, Department of Chemistry, Bangladesh University of Engineering and Technology (BUET), for his kind supervision, indispensable guidance, valuable and constructive suggestions, liberal help, and continuous encouragement during the whole period. His attributive contribution and efforts have greatly shaped me into what I achieved today. I am quite fortunate to be a part of his ambitious research team. I would like to convey my deepest gratitude to Dr. Md. Shakhawat Hossain Firoz and Dr. Chanchal Kumar Roy for their valuable suggestions appreciated comments, guidance, and help during the research period. I am thankful to all other respected teachers of the Department of Chemistry, BUET, for their time-to-time support. I would also like to thank all of the officers and staff of the Department of Chemistry, BUET for their continuous help during my study period. I am highly grateful to all members of the board of examiners for their valuable suggestions and appreciated comments. I am thankful to my dear fellows and all the members of my Research Group for their friendly cooperation and lovely encouragement throughout my research period. Special thanks to Md. Akter Hossain Reaz, Md. Yeasin Arafat Tarek, Pranta Protik, Asif Hasan, Hridoy Roy, Md. Mahmudul Hasan Rumon, Sanjida Afrin, Md. Rabiul Hasan, Md. Anwarul Azim Akib, Keya Chowdhury, and Maherun Negar Majumdar for their continuous help during the research. I am grateful to the authority of BUET, UGC, and the ministry of Science and Technology for financial support in this research. Finally, I would like to express my heartfelt indebtedness and profound gratitude to my beloved mother, brother Fahim Shakil and all my family members for their continuous inspiration and immeasurable sacrifices throughout the period of my study.

April 27, 2022 .....

(Ragib Shakil)

Abstract

Currently, supercapacitors are being highlighted for their high-power densities and cycle lifetimes, which enable them to charge and discharge faster than batteries and for a longer period of time. However, the energy density of supercapacitors falls short of that of batteries. By exceeding the operating voltages of standard aqueous and organic electrolytes, room temperature ionic liquids (ILs) may be one approach to increase energy density. Unfortunately, because of their intrinsically high viscosities, ILs have very low conductivities and must be used with caution. Organic solvent dilution has been proven to increase device rate performance even in the most viscous ionic liquids used in electrochemical applications. But the dilution of ILs with water is still under research. The competing effects of both ionic and electronic transport, as well as porosity, make it difficult to thoroughly analyze the effect on devices. This work utilizes cyclic voltammetry, galvanostatic charge-discharge, and impedance spectroscopy in a model system to gain more insight into how dilution with water influences the properties and interfacial behavior of one IL ($[Bmim]^+Cl^-$) with reduced graphene oxide (rGO) electrode. The surface properties and porosity of rGO are characterized by FTIR, XRD, FESEM, and EDX spectroscopy. However, a maximum in both ionic conductivity and intrinsic capacitance is observed at a concentration of 0.5 M $[Bmim]^+Cl^-/H_2O$, suggesting that previously seen changes in bulk properties with dilution are also accompanied by a change in the capacitive behavior of the interface. It is speculated that this maximum in intrinsic capacitance is attributed to both the increased dissociation of ions, as well as the tendency of solvent molecules to screen the electrostatic interactions between ions. Further measurements in devices with rGO electrodes indicate that dilution drastically improves the rate performance of IL-based devices but was unable to exceed an operating potential of 2.4 volts, indicating that impurities are a major issue in this two-component system. A specific capacitance of 324 F g^{-1} with an energy density of 47 Wh kg^{-1} was found in 1 A g^{-1} current density. The supercapacitor with diluted IL and rGO electrodes also showed a 97 % coulombic efficiency with a capacity retention of 92 % even after the 10000 cycles at 10 A g^{-1}.

Chapter-1

INTRODUCTION

1.1 Introduction

As fossil fuels become depleted and greenhouse gas emissions have a negative influence on the environment, there has been a rise in the need for sustainable energy sources throughout the globe. We should look forward to renewable energy sources such as solar, hydro, or wind power to alleviate these issues [1]. As a result of these substantial changes in output, the power generated by these renewable energy sources must be effectively stored to provide the world with energy on demand [2]. Batteries and supercapacitors (SCs) are the two most popular electrochemical energy storage technologies due to their high energy and power density [3, 4]. Though Lithium-ion batteries are frequently utilized in consumer devices because of their high energy density (up to 180 Wh kg^{-1}), it generate heat and dendrites owing to slow electron and ion movement, which may pose a significant safety risk when operating at high power [5]. This has led to a number of high-profile failures, including Tesla's electric vehicle and Boeing's Dreamliner airliner. To address these issues, electrochemical capacitors/supercapacitors may supplement or even replace batteries in particular applications due to their high power and quick charging capabilities, as well as their extraordinarily long cycle life (>100 000 cycles) [6–8]. It has led to an increase in demand for quick charging, excellent cycle stability, and high-power density in applications where these features are needed. Examples include supercapacitors in heavy-duty vehicles, hybrid platforms for commercial trucks and busses, load-leveling systems for intermittent renewable energy sources, and storage systems for electric cars and light rail [9]. Because of their lower energy density, commercially available supercapacitors are still much less efficient than batteries (up to 200 Wh kg^{-1}) and fuel cells (up to 350 Wh kg^{-1}) [10].

Thus, supercapacitors' general application has been restricted, and substantial research is undertaken to achieve the energy-storage capabilities of batteries without compromising their power density or cycle stability. In an effort to overcome the problem of poor energy density, the supercapacitor field has developed electrode materials that can hold more charge per unit area. A variety of materials/composite materials (including carbonaceous material, transitional metal oxide and their composites, conductive polymeric materials, etc.) have been used to construct several types of supercapacitors [11-13]. The charge storage process of a supercapacitor differs

depending on the character, size, and shape of the electrode material. Supercapacitors' electrochemical performance may be improved by using redox-active metal compounds, such as oxides and hydroxides that store charge via reversible changes in valence in redox interactions with electrolytes but suffers from low cyclic stability [14]. Whereas, to store electrical energy, the carbonaceous elements create an electric double Helmholtz layer. The electric double-layer capacitors (EDLCs) are promising energy storage devices because of their quick charging/discharging rate, high power density, and outstanding durability. Many of the most promising possibilities for EDLC are carbon-based materials including graphene, reduced graphene oxides (rGOs), CNTs from biomass-derived porous carbon materials, and activated carbon [15, 16]. The high electrochemical performance of rGO may be related to its morphological perfection, which includes its increased d-spacing and abundant surface area, which makes it unique among them. The energy density of a supercapacitor's electrode is reflected in its storage capacity. Electrode materials' energy storage capacity is directly related to their energy density. Nanostructure stability, surface area, conductivity, and other morphological attributes are all linked to storage capacity. As a result, the utmost research has been done on rGO as a carbonaceous material for EDLC production. But there are certain drawbacks to rGO-based electrode materials for supercapacitors, including their uncontrolled stacking layer creation, which isn't ideal for electrical charge storage [17]. In spite of its high electrical conductivity and enormous surface area, the rGO produced *via* a chemical process has substantially lower electrical conductivity. Several research have been done to reduce this rGO layer stacking and successfully expanded the rGO layers, also generating pores in the rGO surface. Thus, a large number of electrolyte ions may be stored in the porous rGO structures during charging. In addition, a high energy and power density can be attributed to the dispersion of electrical ions across this porous structure.

However, the energy density of SC is largely dependent on the proper combination of electrolytes used with the specific electrode material [18]. An increased energy density may be achieved by extending the electrochemical potential window by using electrolytes that are well-matched to the electrode. Because mathematically the up gradation of the energy density of electrode material is solely related to its working potential. Researchers are always trying a lot of variations in the electrolyte system and modifying them in different ways to understand and find the suitable electrolyte

combination with the suitable electrode material [19]. The organic electrolytes, which have a working potential of more than 4 V, have long been among the most powerful electrolytes. There is no water splitting event associated with organic molecules, in contrast to aqueous electrolytes (acid, base, or neutral). As a result, unlike in aqueous electrolytes, no oxygen or hydrogen gas development has been seen at voltages greater than 1.23 V [20, 21]. Aqueous electrolytes, on the other hand, are far safer and more cost-effective than organic electrolytes. An electrolyte's working potential is always limited by its water-splitting potential (Na_2SO_4), which in turn limits the system's energy density.

So, many researchers are now interested in ILs as supercapacitor electrolytes because they have the potential to expand the operating voltage window (OVW) and provide better energy densities, all while having low vapor pressure and thermal stability [22]. However, because of their high viscosity and low ion conductivity (as low as a few $mScm^{-1}$), these materials may have lower supercapacitor power densities. The viscosity of ILs may be greatly lowered while the ion conductivity is improved by the addition of molecular solvents such as water. To make matters better, since ILs are very water-soluble, they may create strong O-H bonds rather than weak hydrogen bonds when they are hydrated with water, which might reduce the O_2-H_2 evaluation and therefore broaden the possible window for ILs/water electrolytes [23]. The size of anions and cations affects the conductivity of an IL, thus choosing the right one is critical. For instance, 1-butyl-3-methyl-imidazolium chloride ($[Bmim]^+Cl^-$) based ILs offer higher capacitances than other ILs due to their lower anionic size which fits the pore size of the supercapacitor rGO electrode [24]. Thus, it appears that the diluted, $[Bmim]^+Cl^-$ with water could be a potential electrolyte for next-generation supercapacitors giving enhanced capacitance with improved energy and power densities of EDLCs. Inspiring by the aforementioned exciting findings, we herein explored $[Bmim]^+Cl^-$ as a supercapacitor electrolyte and evaluated the performance with the rGO electrode synthesized by improved Hummer's method. The electrochemical performance of the reported rGO-based supercapacitor was evaluated neat $[Bmim]^+Cl^-$ electrolyte, which exhibits optimal performance. Subsequently, the effects of dilution of $[Bmim]^+Cl^-$ with water on the energy storage performances of the rGO-based supercapacitor were studied.

1.2 Objectives of the Present Work

The main objectives of this work are to-

(i) synthesize reduced graphene oxide (rGO) as an active supercapacitor electrode from graphene oxide (GO) through improved Hammer's method and investigate the morphology of the synthesized rGO.

(ii) investigate the effect of dilution of $[Bmim]^+Cl^-$ with water to design optimized ILs/water combinations for rGO-based supercapacitor in pure and diluted $[Bmim]^+Cl^-$ media.

(iii) examine the electrochemical capacitive performances of rGO-based EDLC using $[Bmim]^+Cl^-$ electrolytes by cyclic voltammetry (CV), galvanostatic charging-discharging (GCD), electrochemical impedance spectroscopy (EIS), and cyclic stability.

References

[1] Bueno, C., & Carta, J. A. (2006). Wind powered pumped hydro storage systems, a means of increasing the penetration of renewable energy in the Canary Islands. *Renewable and sustain able energy reviews*, *10*(4), 312-340.

[2] Chu, S., & Majumdar, A. (2012). Opportunities and challenges for a sustainable energy future. *nature*, *488*(7411), 294-303.

[3] Zhang, F., Zhang, T., Yang, X., Zhang, L., Leng, K., Huang, Y., & Chen, Y. (2013). A high-performance supercapacitor-battery hybrid energy storage device based on graphene-enhanced electrode materials with ultrahigh energy density. *Energy & Environmental Science*, *6*(5), 1623-1632.

[4] Olabi, A. G., Abbas, Q., Al Makky, A., & Abdelkareem, M. A. (2022). Supercapacitors as next generation energy storage devices: Properties and applications. *Energy*, *248*, 123617.

[5] Ghiji, M., Novozhilov, V., Moinuddin, K., Joseph, P., Burch, I., Suendermann, B., & Gamble, G. (2020). A review of lithium-ion battery fire suppression. *Energies*, *13*(19), 5117.

[6] Gelb, J., Finegan, D. P., Brett, D. J., & Shearing, P. R. (2017). Multi-scale 3D investigations of a commercial 18650 Li-ion battery with correlative electron-and X-ray microscopy. *Journal of Power Sources*, *357*, 77-86.

[7] Balaji, T. E., Tanaya Das, H., & Maiyalagan, T. (2021). Recent trends in Bimetallic Oxides and their composites as electrode materials for Supercapacitor applications. *ChemElectroChem*, *8*(10), 1723-1746.

[8] Li, Y., Han, X., Yi, T., He, Y., & Li, X. (2019). Review and prospect of NiCo2O4-based composite materials for supercapacitor electrodes. *Journal of energy chemistry*, *31*, 54-78.

[9] Afif, A., Rahman, S. M., Azad, A. T., Zaini, J., Islan, M. A., & Azad, A. K. (2019). Advanced materials and technologies for hybrid supercapacitors for energy storage–a review. *Journal of Energy Storage*, *25*, 100852.

[10] Zhao, X., Sánchez, B. M., Dobson, P. J., & Grant, P. S. (2011). The role of nanomaterials in redox-based supercapacitors for next generation energy storage devices. *Nanoscale*, *3*(3), 839-855.

[11] Kumar, A., Rathore, H. K., Sarkar, D., & Shukla, A. (2021). Nanoarchitectured transition metal oxides and their composites for supercapacitors. *Electrochemical Science Advances*, e2100187.

[12] Choi, J. H., Lee, C., Cho, S., Moon, G. D., Chang, H., & Jang, H. D. (2018). High capacitance and energy density supercapacitor based on biomass-derived activated carbons with reduced graphene oxide binder. *Carbon*, *132*, 16-24.

[13] Bandosz, T. J., & Ren, T. Z. (2017). Porous carbon modified with sulfur in energy related applications. *Carbon*, *118*, 561-577.

[14] Yan, J., Wang, Q., Wei, T., & Fan, Z. (2014). Recent advances in design and fabrication of electrochemical supercapacitors with high energy densities. *Advanced Energy Materials*, *4*(4), 1300816.

[15] Wang, W., Luo, Q., Li, B., Wei, X., Li, L., & Yang, Z. (2013). Recent progress in redox flow battery research and development. *Advanced Functional Materials*, *23*(8), 970-986.

[16] Al-Shara, N. K., Sher, F., Iqbal, S. Z., Curnick, O., & Chen, G. Z. (2021). Design and optimization of electrochemical cell potential for hydrogen gas production. *Journal of Energy Chemistry*, *52*, 421-427.

[17] Bak, T., Nowotny, J., Rekas, M., & Sorrell, C. C. (2002). Photo-electrochemical hydrogen generation from water using solar energy. Materials-related aspects. *International journal of hydrogen energy*, *27*(10), 991-1022.

[18] Ivol, F., Porcher, M., Ghosh, A., Jacquemin, J., & Ghamouss, F. (2020). Phenylacetonitrile ($C_6H_5CH_2CN$) ionic liquid blends as alternative electrolytes for safe and high-performance supercapacitors. *Molecules*, *25*(11), 2697.

[19] Crawford, B. (2020). Elucidating the Properties and Mechanism for Cellulose Dissolution in Tetrabutylphosphonium-Based Lonic Liquids Using High Concentrations of Water. West Virginia University.

[20] Correia, D. M., Fernandes, L. C., Martins, P. M., García-Astrain, C., Costa, C. M., Reguera, J., & Lanceros-Méndez, S. (2020). Ionic liquid–polymer composites: A new platform for multifunctional applications. *Advanced Functional Materials*, *30*(24), 1909736.

[21] Alipour, S., & Mousavi-Khoshdel, S. M. (2019). Investigation of the electrochemical behavior of functionalized graphene by nitrophenyl groups as a potential electrode for supercapacitors. *Electrochimica Acta*, *317*, 301-311.

[22] Tjandra, R., Liu, W., Lim, L., & Yu, A. (2018). Melamine based, n-doped carbon/reduced graphene oxide composite foam for Li-ion Hybrid Supercapacitors. *Carbon*, *129*, 152-158.

[23] Roy, C. K., Shah, S. S., Reaz, A. H., Sultana, S., Chowdhury, A. N., Firoz, S. H., & Aziz, M. A. (2021). Preparation of Hierarchical Porous Activated Carbon from Banana Leaves for High-performance Supercapacitor: Effect of Type of Electrolytes on Performance. *Chemistry–An Asian Journal*, *16*(4), 296-308.

[24] Ivol, F., Porcher, M., Ghosh, A., Jacquemin, J., & Ghamouss, F. (2020). Phenylacetonitrile ($C_6H_5CH_2CN$) ionic liquid blends as alternative electrolytes for safe and high-performance supercapacitors. *Molecules*, *25*(11), 2697

Chapter-2

BACKGROUND CONCEPTS

2.1 Background of Supercapacitor

Helmholtz initially established the idea of "double-layer capacitance" in 1853, which corresponds to the charge storage at the electrode-electrolyte interface [1]. However, there was no use of this finding during that time span [2]. The first electric double-layer capacitor (EDLC) with carbon electrodes and an aqueous electrolyte was patented by Becker in 1957 [3]. Carbon electrodes with tetraalkylammonium salt electrolyte were invented by the Sohio Corporation (Cleveland) in 1962, and the company was given an EDLC patent. A computer memory backup device called the "Supercapacitor" was first offered to the market by Nippon Electric Company (NEC) in 1971 [4]. For electrochemical capacitors based on ruthenium oxide, a novel concept known as "pseudocapacitance" was developed by Conway et al. between 1975 and 1983, including rapid and reversible Faradaic processes (redox reactions) on the electrode surfaces [5]. Double-layer capacitors, such as Panasonic's "Goldcaps" and Pinnacle Research Institute's "PRI Ultracapacitor," were made in the 1980s by a number of businesses. Prior to Maxwell Laboratories' acquisition of PRI research in 1992, the moniker "Pri" was known as "Boost Caps." The specific energy, specific power, and cycle life of supercapacitors are being improved by universities, research centers, and enterprises today.

2.2 Difference Between SC and Battery

SCs and batteries have been widely explored however there is significant misunderstanding and misleading between them in publications. In particular, several battery characteristics are erroneously called supercapacitors and some claimed “remarkable” results as the high specific capacitance of 2188 F g^{-1} for $Ni(OH)_2$ nanospheres are not accurate. It is conceivable that the energy storage method and the related device configuration/characterization procedures produce confusion. It is necessary to explain and eliminate misconceptions concerning both theoretical and experimental elements of these two kinds of energy devices.

Figure 2.1 shows a Ragone chart that compares the specific power and specific energy of different types of capacitors and batteries. Here, we can see the SCs bridge the gap between batteries and traditional solid-state and electrolytic capacitors, but they are usually limited by their relatively low energy density. Energy-packed batteries, like lithium-ion batteries with a range of 100–265 Wh kg^{-1}, have more energy per unit weight, but they suffer from low power density [6]. Usually, the SCs have energy density below 20 Wh kg^{-1} and power density above 10 kW kg^{-1} [7]. This is usually 10 to 100 times more than the batteries [7]. These four energy storage devices shown in Figure 2.1 aren't the only ways to store energy. Conventional gasoline and hydrogen combustion engines can reach very high specific power density and energy density, even though these internal combustion engines use fossil fuels which is the main reason for CO_2 emission and global warming issues. The energy density and power density of both the battery and the SCs are still a long way off from fossil fuels, but they're getting there. This means that for SCs and batteries, the big goal is to make them powerful and have a high energy density, which is the "question" marked goal in Figure 2.1.

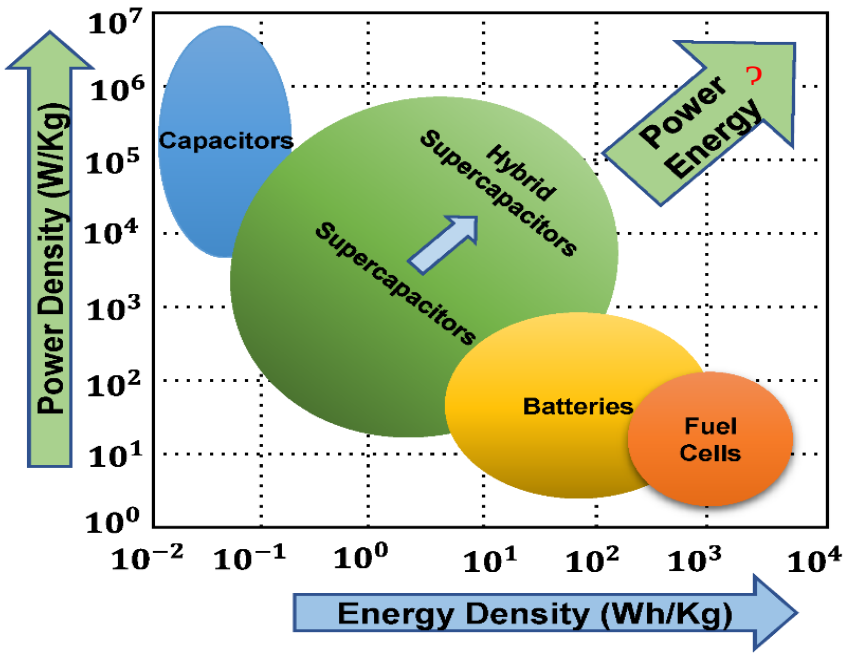

Figure 2.1. Position of battery and supercapacitor in Ragone plot

2.3 Supercapacitors Classification

With respect to their device design, electrochemical capacitors are quite similar to batteries, with two electrodes separated by an ion-permeable membrane (separator) and connected by an electrolyte acting as an ion-conducting path between them. An illustration of typical SC components is shown in Figure 2.2

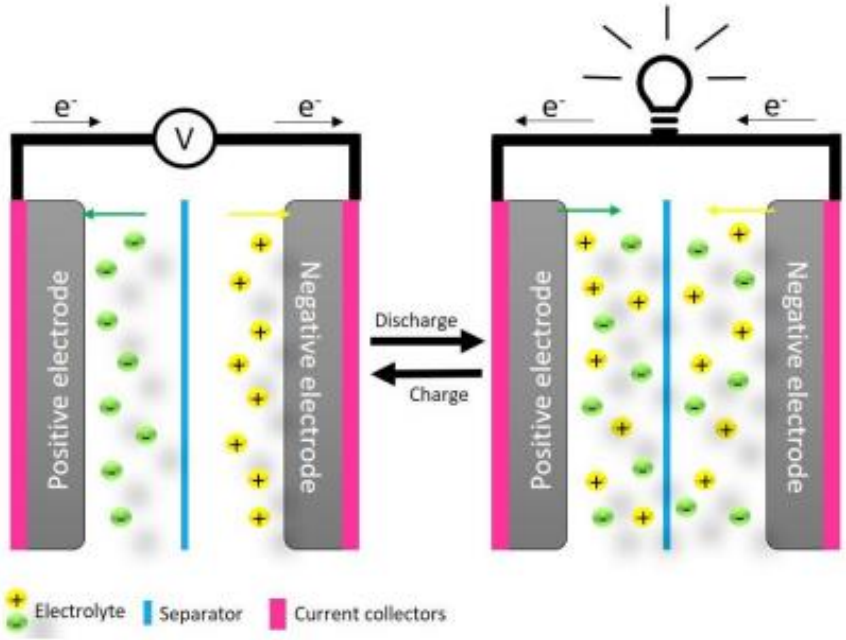

Figure 2.2. Typical SCs components; charging (left) and discharging (right)

Supercapacitors are classified into two types based on their charge storage techniques and the active material utilized as electrodes. Both classes may be combined into one since they are connected, *i.e.*, the energy storage technique can vary based on the electrode material used. As a result, supercapacitors may be categorized into three types based on their charge storage and release mechanism: (i) electrical double-layer capacitor (EDLC), (ii) pseudocapacitor, or electrochemical supercapacitor (ES), and (iii) hybrid supercapacitor (HS) [8]. Each group may be further split according to the active materials used, as seen in Figure 2.3.

EDLC is a method of storing electrical charge electrostatically at the electrode-electrolyte interface by the reversible adsorption/desorption of ions at the electrode-

electrolyte interface when carbon-based electrodes are used [9]. Faradaic reactions, which occur quickly and reversibly on the electrode surface, allow ES based on electrically conducting polymers or transition metal oxides to store charge on the electrode surface. EDLC and ES processes are combined in a single device in the case of hybrid supercapacitors, which means that the charge is held both electrostatically and electrochemically in a single device [10].

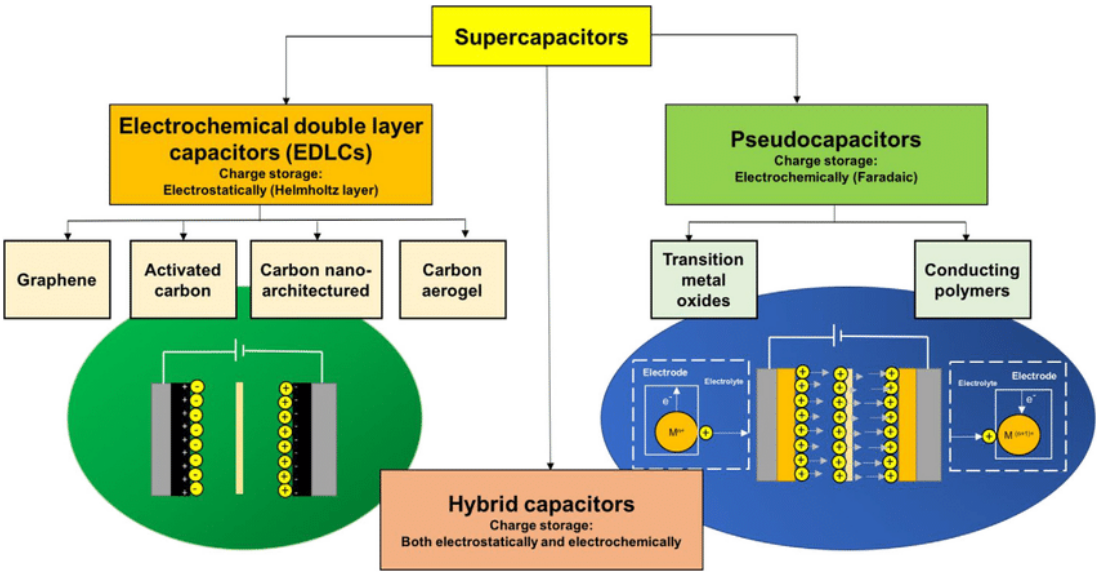

Figure 2.3. Classification of supercapacitors

Aside from the classification explained above, supercapacitors can be symmetric or asymmetric depending on the electrodes used for assembly [11], *i.e.*, a symmetric supercapacitor is formed by assembling two electrodes with the same composition as positive and negative electrodes, whereas an asymmetric supercapacitor is formed by assembling two electrodes with different composition as positive and negative electrodes. For example, a battery type electrode as the energy source and a capacitor type electrode as the power source [12], such as the lithium-ion capacitor (LIC), which is an asymmetric hybrid device [13] due to the combination of a battery mechanism in the negative electrode (lithium titanate) and an electric double-layer supercapacitor mechanism in the positive electrode (activated carbon) [14].

2.4 What are the EDL-based SC?

In a supercapacitor, electrical charge may be stored electrostatically or electrochemically, as described in the preceding section. The electrical double-layer capacitance mechanism and the pseudocapacitance mechanism are both ways of storing charge. The pure carbonaceous material stores charges by forming an electric double layer (EDL) in between the electrode and electrolyte interface thus also termed EDL-based SC.

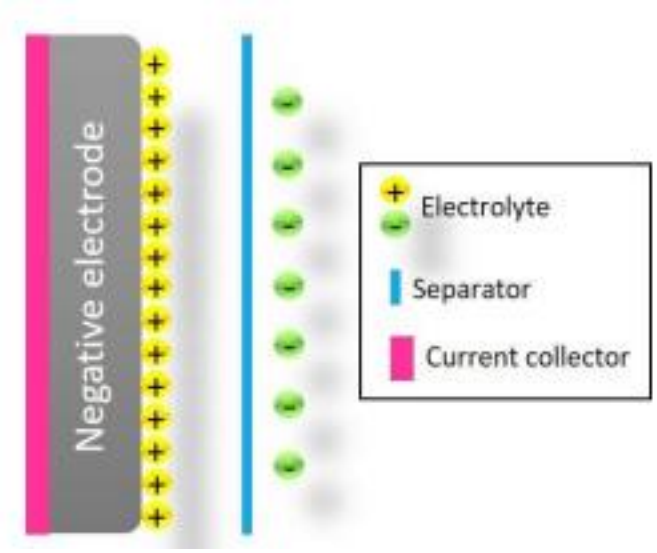

Figure 2.4. Scheme of the compact electrical double-layer described by the Helmholtz model

In 1879, Helmholtz's presented a model that describes the EDL formation in an SC during the charging/discharging process [15]. The EDLCs functioning principles may best be grasped using this EDL model, as it is the most simplistic. Electrode-electrolyte interaction results in the formation of the "electrical double-layer," as seen in Figure 2.4 when the two conductors are in close proximity to each other.

After that, a number of models have been developed as a result of the Helmholtz model (compact layer), and these models explain in more detail the probable construction of the "electrical double-layer," including diffusion in solution and interaction of the

solvent with the electrode surface [16]. The Gouy-Chapman model (which includes a diffuse double-layer), the Stern model (which combines the compact and diffuse double-layers), and the Bockris-Devanathan-Müller (BDM) model, which includes the solvent action at the electrode interface [17]. As shown in Figure 2.5, the BDM model is the most detailed, and it states that there is a first layer formed at the electrode surface known as the inner Helmholtz plane (IHP), which refers to the monolayer of the polarized solvent molecules, and a second layer corresponding to the charge layer in the electrolyte that is known as the outer Helmholtz plane (OHP), which refers to the charge layer in the electrolyte [18]. The orientation and permittivity of the solvent molecules, according to this hypothesis, are both substantially dependent on the electric field applied to them.

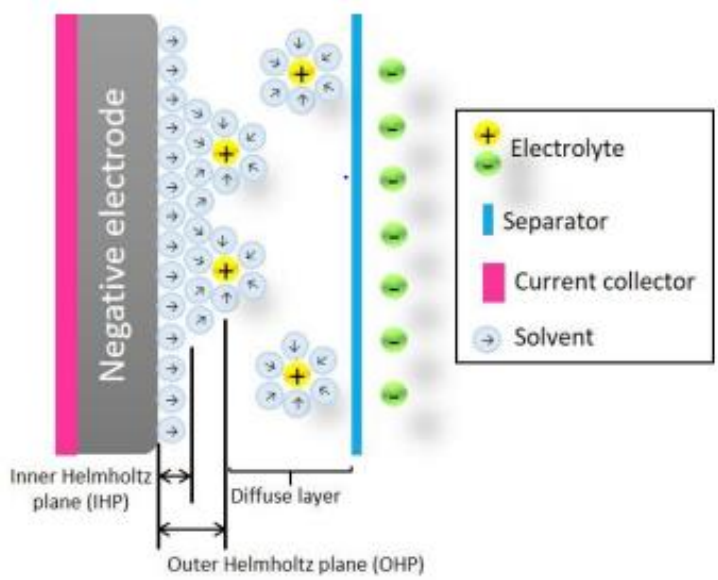

Figure 2.5. Schematic view of a double-layer between a negative electrode surface and an electrolyte by the BDM model

For SCs, the electrode materials are one of the critical elements in determining their performance including the capacitance, rate capability, and cycle life stability. As a result, various carbonaceous materials such as activated carbon, carbon aerogels (CAGs), graphene (GO, rGO), CNTs, carbon nanofibers (CNFs), and nanosized carbon have been widely investigated and reported for developing the EDL-based SCs electrode/EDLCs [19]. These electrode materials have been actively studied because of their accessibility, ease of processing, low cost, non-toxicity, high chemical

stability, and wide temperature range. Different methods have been used to raise the specific surface area (SSA) of these materials or to alter the pore size distribution (PSD). As a consequence, the energy, power, and operating characteristics of SCs have significantly improved. Because of its high SSA and low price, activated carbons are now the most often utilized material [20-22]. In organic electrolytes, these materials have exhibited capacitance values of between 150 and 300 F g^{-1}, and between 100 and 120 Fg^{-1}, in aqueous electrolytes. As a result of water breakdown, a reduced operating voltage may be detected in the latter [23]. There is a significant amount of research being done to enhance the energy density of supercapacitors by developing carbon-based electrode materials without sacrificing their high-power delivery and cycle life.

2.5 rGO-Based Supercapacitor

One of the most remarkable aspects of the 2-D carbon monolayers known as Graphene is its lightweight, high electrical and thermal conductivities, highly adjustable surface area (up to 2675 $m^2 g^{-1}$), and great mechanical strength (~1 Tpa), as well as its chemical stability [24]. Graphene and graphene-based materials may be used in high-performance structural nanocomposites, electronics, environmental protection, and energy devices, including both energy production and storage, because of these exceptional qualities they possess. graphene-based materials are increasingly desirable for electrochemical energy storage and sustainable energy production, including Li-ion batteries, fuel cells, supercapacitors, and photovoltaic and solar cells because of their remarkable physical and mechanical qualities. Single-layer graphene, for example, has a theoretical specific capacitance of around 21 uF cm^{-2}, and the equivalent specific capacitance is 550 F g^{-1} when the whole surface area is used [25].

However, in the graphene family, graphene oxides (GOs) are an additional key component. They have the layered structure and surface-related characteristics of graphite, which can be easily synthesized. GO may have a variety of surface groups and distributions depending on the synthesis method used. Some functional groups

with oxygen, such as hydroxyl (C-OH), carboxyl (C=O), and epoxy groups, attach to the edges of GO sheets and help to keep them stable in their quasi-two-dimensional form [26, 27]. Different reduction techniques easily transform GO into graphene sometimes called rGO. The reduction of GO is shown in Figure 2.6 using chemical methods. The oxidation of natural graphite may produce GO, a precursor to graphene, in vast quantities and at a minimal cost.

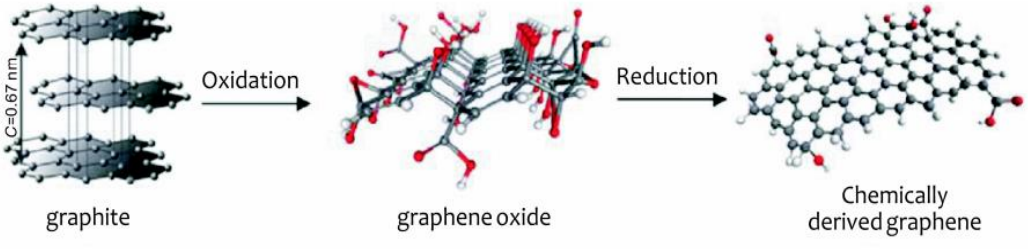

Figure 2.6**.** Illustration of the chemical route to the chemically derived graphene/rGO

When it comes to generating graphene, the reduction of GO is an inexpensive process. Atomic layers of graphene oxide (GO) typically include phenol epoxy and epoxide groups on the basal plane and ionizable carboxylic acid groups on the edges. The acid groups on the ionized edge allow for the stability of GO in the aqueous dispersion in the form of a single-sheet layer *via* weak dipole and quadrupole van der Waals interactions with the surrounding environment, resulting in the formation of a single-sheet rGO layer [28]. Due to its high degree of processing and dispersion capabilities in solution, GO provides a practical way for creating graphene/rGO on a wide scale that has been sought. Due to significant agglomeration occurring during the preparation and application operations, the actual capacitive behavior of rGO is lesser than expected. As a result, scientists have explored many ways to improve their electrochemical performance.

A granular MnO_2/graphene composite was created by Li's team utilizing the previously synthesized graphene, $KMnO_4$, and K_2SO_4 as basic materials [29]. The electrochemical characteristics of the composite electrode were investigated using cyclic voltammetry and electrochemical impedance spectroscopy, with the electrolyte being a 1 M Na_2SO_4 aqueous solution [30]. When the potential scanning rate is 2 mV s^{-1}, the specific capacitance value of the electrode reaches 211.5 F g^{-1}, and the electrode

exhibits excellent cycling performance as well as a high specific capacitance value [31]. An in-situ polymerization of aniline monomers, carried out by Wu's team at the National University of Singapore, was the first to reveal that chemically modified graphene and polyaniline nanofiber composites could be synthesized under acidic circumstances utilizing aniline monomers [32]. In this study, graphene oxide/polyaniline (PANI) composites were reduced to rGO by hydrazine, and then the reduced PANI was reoxidized and reduced to generate rGO/PANI nanocomposites. Under the conditions of 0.1 A g^{-1} charging current, the specific capacitance of the resultant material is 480 Fg^{-1}, which is quite high. This homogeneous structure, in combination with the observed high conductivity, results in a high specific capacitance and strong cycle stability, which are both beneficial [32]. Zhang et al. used Ni foam as a sacrificial template in a simple CVD procedure using ethanol as a carbon source to create 3-D rGO network. The graphene rGO-NiO 3-D nanocomposites for supercapacitor electrodes were constructed using the superior templates provided by the 3-D graphene networks [33]. Fast electron transfer between active materials and current collectors in supercapacitors is made possible by the high conductivity and large specific surface area of rGO, which are practically as good as those of pristine graphene. An 816 Fg^{-1} specific capacitance and robust cycling performance of the rGO-NiO 3-D nanocomposite after 2000 cycles have been shown [33].

Electrochemical energy storage technologies, such as SCs, may benefit greatly from the use of rGO as electrode materials. There has been a lot of progress in recent years in the design, manufacture, performance assessment, and understanding of major electrochemical processes seen [34-36]. If full-scale practical use is to be realized, electrode materials' quality and repeatable quantity must be significantly enhanced, with the production of the most desirable shapes adjustable at nano, micro, meso, and macro sizes in particular. This is a huge task. Exfoliating graphite into GO and reducing it to rGO is the cheapest and most efficient way to make graphene-based products [37]. However, stabilization of single or few-layer graphene sheets in various solvents and the preservation of their intrinsic properties must be addressed before large-scale application of this simple processing method in electrochemical energy storage devices to break the bottleneck of re-stacking of graphene/rGO [38].

2.6 An Insight view of Supercapacitor Electrolyte

It is the active materials used that set the energy output possible for any supercapacitor and such attracts more attention. But, to extract maximum benefits from electrode materials, researchers are also focusing on the electrolyte side to improve the operating voltage window (OVW) of EDLCs [39]. Hence, it has gathered great attention to developing some novel electrolytes to improve SCs performance. The effects of the electrolyte on the SC performance are shown in Figure 2.7. According to E_{qn} 1, the electrochemical stability potential (V) of the electrolyte has a direct link with the amount of energy stored in the SC [40].

$$E = \frac{1}{2} CV^2 \quad (1)$$

Macroscopically, physical features of electrolytes are also critical for a high-performing SC device like a low wettability of the SC electrode by the electrolyte results in low ionic conductivities with higher equivalent series resistance (ESR) values [41]. The transition temperatures (boiling, melting, glass transition, and flash points) of the electrolyte are critical in determining the operating temperature range of the supercapacitors, and their safety is largely dependent on their flash points (the lowest temperature at which a volatile material can vaporize to form an ignitable mixture in the air) [42]. The conductance and dissociation of the ions in the electrolyte govern the performance of the supercapacitor, which in turn is influenced by the following variables:

- Solubility of the salt or acid
- Degree of dissociation or extent of cation and anion pairing in solution
- Dielectric constant of the bulk solvent
- Electron pair donicity of the solvent molecules
- Mobility of the free, dissociated ions
- Viscosity of the solvent
- Solvation of the free ions and the radii of the solvated ions
- Temperature coefficient of viscosity and of ion-pairing equilibria
- Dielectric relaxation time of the solvent

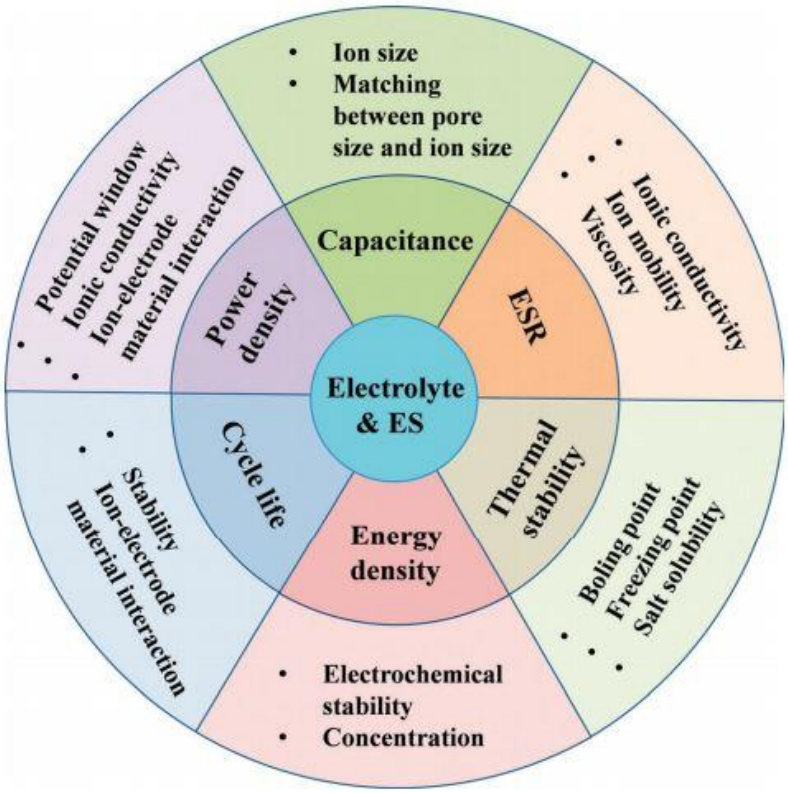

Figure 2.7. Effects of electrolyte on SCs.

To enhance the energy density of SC different electrolytes, such as organic, aqueous, ionic liquid (IL), redox-type, and solid or semi-solid electrolytes, have been investigated, and considerable progress has been made during the past several decades [43-45]. Various categories of electrolytes for SC are shown in Figure 2.8. Non-aqueous solvent-based organic electrolytes (OEs) and ILs significantly improved the supercapacitor's performance. The OEs and ILs-based supercapacitors can easily obtain a large potential window of 2-3 V and 3-5 V, respectively [46]. However, organic electrolytes typically suffer from flammability, volatility, and toxicity. Most importantly, sluggish ion diffusion is usual for the high viscosity of OEs [47]. Although ILs can overcome these limitations, but their non-availability and expensiveness have limited further application in supercapacitors. Here, aqueous electrolytic systems are most preferable because of their high ionic conductivity, non-volatility, non-flammability, and inexpensiveness. Nevertheless, limited by the narrow operating potential window due to hydrogen and oxygen evolution reactions, thus having low energy densities [48]. In many cases, aqueous electrolyte preconditioning

in the highly pure state is not facile for large-scale applications in supercapacitors. That is why the search for available and efficient electrolytes for supercapacitors has gained significant attention.

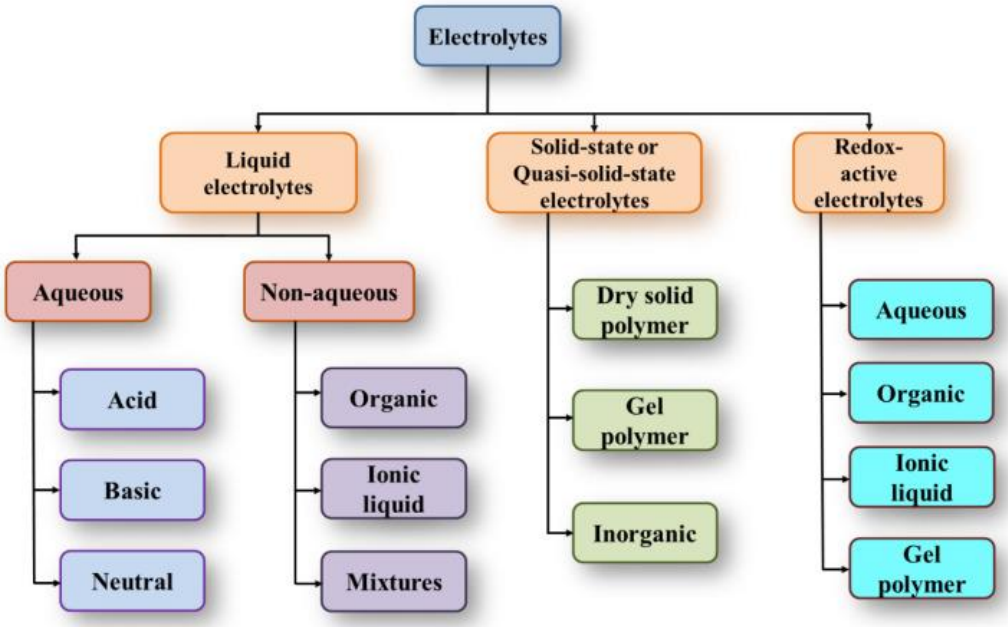

Figure 2.8. Classification of electrolytes for SC.

2.7 Requirements for Designing Electrolytes for SCs

2.7.1 Electrolyte conductivity

Electrolyte plays a vital role in increasing *E, P, and* cyclic stability of SC. Conductivity and ionic mobility of an electrolyte are essential factors to consider when evaluating their efficiency. Since aqueous electrolytes have a low dynamic viscosity, their conductivity is usually higher than that of non-aqueous/OEs/ILs and solid electrolytes [49]. The conductivity (σ) of an electrolyte can be expressed by E_{qn} 2 [50].

$$\sigma = \Sigma\, n_i\, \mu_i\, z_i\, e \qquad (2)$$

Here, σ is the conductivity of species, (μ_i) is the ionic mobility, (n_i) is the charge carrier concentration, (e) is the elementary charge, and (z_i) is the valence of mobile ion charges.

The coefficients shown in this equation are affected by the solvation effect, ion migration, and salt lattice energy. As a result, the conductivity of an electrolyte can be influenced by all constituents, including solvents, additives, and salts.

2.7.2 Salt effect

Because of the interaction between the anion and the cation, as well as the volume difference of various anions, the conductivity of different salts in the same solvent can vary. So, in the context of the conductivity of an electrolyte, the mobility and concentration of ions play a significant role [51]. At a lower concentration the number of the free ions is superior, so the optimum salt concentration can enhance the electrolytes conductivity. The conductivity of an electrolyte will be highest when the viscosity and free ions are in equilibrium condition. When the salt concentration in the solvent is high, the anions and cations in the solvent form tight bonds with the neutral ions, reducing the number of free ions and lowering the electrolyte conductivity. The conducting salts also have a significant impact on the potential window and capacitance of SCs. Several factors such as solubility, conductivity, and cost should be considered when selecting suitable salts for some solvents. However, in a viscous ionic liquid system, the conductivity decreases with the increase in solution concentration [52].

2.7.3 Electrochemical stability

The cycling life of SC is closely linked to the electrolyte’s electrochemical stability. The electrochemical stabile window or potential window of an electrolyte is described by the upper and lower limits of redox reactions in electrolytes. The electrochemical stability can not only be determined by the electrolyte's constituents, but it also depends on the electrolyte's compatibility with the electrode. Despite certain variations

in testing outcomes by using several test devices, cyclic voltammetry is the most widely used measurement technique to measure the electrochemical stability. The electrochemical stability highly depends on temperature. With the variation in temperature, the electrochemical stability can change. It's crucial to conduct a thorough investigation into the electrochemical stability of electrolytes at different temperatures. Some literature reviewed that electrode material, salt type, and solvent system affect the electrochemical stability [53, 54].

2.7.4 Thermal stability

During the charging-discharging process, some electrolytes are vulnerable to decomposition, which is linked to a rise in operating temperature and heat release, and this rise in temperature causes safety issues for the SCs [55]. As a result, the supercapacitor electrolyte's thermal stability is an important parameter to investigate. The interaction of the electrolyte and electrode with each other, as well as the thermal stability of the electrolyte itself, determine the thermal stability of SCs. An electrolyte's thermal stability is primarily determined by its composition, which includes salt, solvent, and any additives [56]. TGA/DSC tests are commonly used to investigate it.

2.8 Ionic Liquids as Supercapacitor Electrolyte

Increasing the cell voltage of EDLC to more than 3 V is a hot topic in the industry [57-59]. The electrochemical stability window of organic solvents shrinks with rising temperature, and an increase in maximum cell voltage also diminishes the cycle life of EDLCs, thus they would be unable to live up to their cyclability reputation under these circumstances. As a result, ILs, which are renowned for their broad electrochemical stability as well as their high thermal stability, are being extensively explored for the reasons stated above [60].

2.8.1 Brief historic evolution of molten salts to ILs

Salts in the liquid phase are known as molten salts; nevertheless, at ordinary temperatures and pressures, salts generally reside in the solid phase (STP) [61]. However, under normal temperature and pressure salts remain in the solid-state in the form of molten salts (STP). The electrochemical reduction of aluminum (III) in molten cryolite (Na_3AlF_6) at 980 °C yields elemental liquid aluminum. Due to thermal stability and non-volatility, molecular media do not allow for a large liquidus range. Eutectic mixture of LiCl–KCl has a melting point of 355 °C, but the working temperatures remain high, making it difficult to carry out reactions on any scale without encountering major material incompatibilities and incurring substantial energy expenditures to sustain the high temperature [62]. In 19-14, $EtNH_3[NO_3]$ became the first practical low-melting salt (Ionic liquid) (12 ^oC) [63]. It was only later that triethylammonium nitrate appeared in the 1930s for dissolving cellulose at temperatures exceeding 130 ^oC [64]. Molten N-ethylpyridinium chloride was initially identified in the 1930s (Graenacher, 1934) as a solvent for cellulose [65]. This result, however, received very little attention at the time. This so-called "red oil" was originally seen by chemists in the mid-19th century when they observed the reaction of benzene with chloromethane to create toluene, generally in the presence of a Lewis acid catalyst like $AlCl_3$ [66]. In the late 1940s, Hurley and Weir at Rice University researched N-alkylpyridinium chloroaluminates as electrolytes for electroplating aluminum. During the late 1970s, more study was supported by Hussey, Osteryoung, and Wilkes [67]. $[EMI]^+Cl^-$ and aluminum trichloride were used by Wilkes and colleagues in the early 1980s to produce one of the first 1,3-dialkylimidazolium room temperature ionic liquids (RTILs) [68]. However, the hydrophilic character of chloroaluminate anion and its strong reactivity toward water restrict the uses for this organo-aluminate IL.

Imidazolium-based ILs were discovered in the 1990s, such as 1-ethyl-3-methylimidazolium tetrafluoroborate (Emi-BF_4), by Wilkes and colleagues, and 1-ethyl-3-methylimidazolium hexafluorophosphate (Emi-PF_6), by Fuller and colleagues [69]. Since then, the $[Emi]^+$ cation has sprung into the search for numerous uses,

leading to the rediscovery of molten salts. By far the most extensively investigated halogenoaluminate (III) until 2001 was $EmiAlC_4$, followed by the closely related alkylhalogenoaluminate (III) IL [70]. Imidazolium salts have remained one of the most well studied RTILs, including the discovery that cellulose may be effectively dissolved at low temperatures (less than 100 °C) in imidazolium based ILs. Non-aromatic cyclic cations like pyrrolidinium and piperidinium are also becoming prominent cations.

Nowadays, a lot of people have looked into how to use ILs in SCs, both in activated carbon double-layer capacitors and in hybrid polymer supercapacitors [71, 72]. Both activated carbon double-layer capacitors and hybrid polymer supercapacitors have been widely explored for the incorporation of ILs in supercapacitors. There are reports by Balducci et al. that describe the use of microporous activated carbon and an ionic liquid (*N*-butyl-*N*-methylpyrrolidinium bis(trifluoromethanesulfonyl)imide (PYR_{14}-TFSI)) as the electrolyte, resulting in a specific capacitance of 60 Fg^{-1} at a typical scan rate of 20 mV s^{-1} for EDLC and a maximum operating potential range of 4.5 V at 60 °C [73]. Lewandowski et al. employed ILs like Ethyl-3-MethylImidazolium Tetrafluoroborate (Emi-BF_{40}), PYR_{14}-TFSI, and 1-Butyl-3-MethylImidazolium hexafluorophosphate (Bmi-PF_6) electrolytes in hybrid supercapacitors [74]. Zhu et al. utilized Emi-TFSI as an electrolyte for EDLC which was shown to have a capacitance of 200 F g^{-1} at 3.5 V at room temperature [75].

2.8.2 Choice of ILs for SC Electrolyte

Since there are literally millions of potential cation-anion combinations, the composition and related characteristics of IL are highly dependent on the specific combinations that have been found, and this number has been estimated to be as high as 1018 [76]. Alternating anions or alkyl groups of cations may therefore be used to tailor ILs to specific applications. As can be seen in Figure 2.9, the basic building elements of ILs are what provide current electrolytes with a greater degree of diversity (various characteristics).

Fox example, conductivity decreases in the following order for a given anion and a variety of cations: imidazolium > pyrrolidinium > ammonium > pyridinium [77]. This has been explained by a more planar imidazolium cationic core, which results in higher conductivity, as opposed to the bulkier ammonium salts, which have a tetrahedral arrangement of alkyl groups. In terms of electrochemical stability of ILs with regard to the cations follows the order of ammonium, imidazolium, piperidinium, and pyrrolidinium respectively.

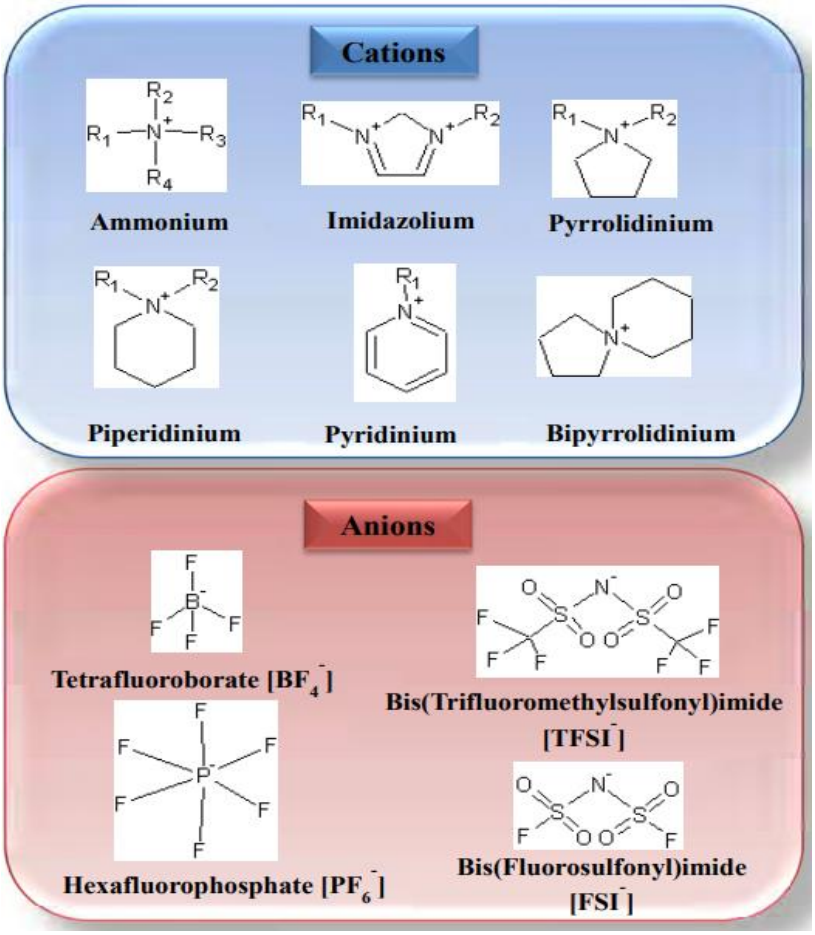

Figure 2.9. Common building blocks of ILs – Cations (Upper panel) and anions (Lower panel). R groups may take on hydrogen atoms or different alkyl groups such as methyl, ethyl, propyl, butyl, etc.

The miscibility of Bmim-PF_6 and Bmim-BF_4 cation salts, for example, is the only difference between the two cation salts; the other characteristics of PF_6^- and BF_4^- salts are almost identical [78]. It is possible to construct a wide range of solvents because

of this difference. EDLC devices' cycle life and performance may be reduced or ruined if their electrolytes get contaminated with water. The presence of water traces in PF_6^- based ILs causes HF at increased temperatures, despite the fact that they are less hydrophilic than BF_4^- based ILs [79]. Whereas the Bmim-Cl is able to retain its properties in the presence of water. So, Cl^-, Br^-, I^-, $TFSI^-$, and FSI^- anions have been used to alleviate this issue [80]. The $TFSI^-$ and FSI^- anions include fluorine, but unlike PF_6^- and BF_4^-, their fluorine atoms are linked to carbon, making the C-F bonds inert to hydrolysis and the formation of HF. These imides and related anions are the basis for the IL now being sold. These fluorinated anions, however, have a tendency to be prohibitively costly when used in large quantities. Thus, researchers are moved to halaid-based ILs as SC electrolytes due to their intrinsic physical properties.

2.9 Regulation of imidazolium based ILs with solvents

Despite the high energy densities offered by the wide electrochemical stability of the ILs, there is always a compromise in the power capability of the EDLCs due to the high resistance incurred owing to the high viscosities and lower conductivities of ILs in general. Attempts have been made [81] by adding solvents such as propylene carbonate (PC) or Acetonitrile (AN) to ILs to improve conductivity (60 mS cm-1 for AN) and eventually power, but it is noteworthy that the electrochemical window which can be accommodated has to be kept within that of AN or PC which in turn limits the energy density capacity. Hence, to fully benefit from the maximum electrochemical stability of RTILs, most reported use of RTILs in EDLCs with porous electrodes are usually at elevated temperatures of $\geq 60°C$ [81] to reduce the electrolyte viscosity, enhance ionic mobility, and thereby keep ESR values low.

References

[1] Iozzo, D. A., Tong, M., Wu, G., & Furlani, E. P. (2015). Numerical analysis of electric double layer capacitors with mesoporous electrodes: effects of electrode and electrolyte properties. *The Journal of Physical Chemistry C*, *119*(45), 25235-25242.

[2] Namisnyk, A., & Zhu, J. (2003). A survey of electrochemical super-capacitor technology. In *Australian Universities Power Engineering Conference*. University of Canterbury, New Zealand.

[3] Sharma, P., & Bhatti, T. S. (2010). A review on electrochemical double-layer capacitors. *Energy conversion and management*, *51*(12), 2901-2912.

[4] Azaıs, P. (2013). Manufacturing of industrial supercapacitors. *Edited by Francois Béguin and Elzbieta Fr şackowiak*.

[5] Xie, J., Yang, P., Wang, Y., Qi, T., Lei, Y., & Li, C. M. (2018). Puzzles and confusions in supercapacitor and battery: Theory and solutions. *Journal of Power Sources*, *401*, 213-223.

[6] Keum, K., Kim, J. W., Hong, S. Y., Son, J. G., Lee, S. S., & Ha, J. S. (2020). Flexible/stretchable supercapacitors with novel functionality for wearable electronics. *Advanced Materials*, *32*(51), 2002180.

[7] Radhamani, A. V., Shareef, K. M., & Rao, M. R. (2016). ZnO@ MnO2 core–shell nanofiber cathodes for high performance asymmetric supercapacitors. *ACS Applied Materials & Interfaces*, *8*(44), 30531-30542.

[8] Farahpour, M., & Arvand, M. (2022). In situ synthesis of advantageously united copper stannate nanoparticles for a new high powered supercapacitor electrode. *New Journal of Chemistry*.

[9] Ahirrao, D. J., Tambat, S., Pandit, A. B., & Jha, N. (2019). Sweet-Lime-Peels-Derived Activated-Carbon-Based Electrode for Highly Efficient Supercapacitor and Flow-Through Water Desalination. *ChemistrySelect*, *4*(9), 2610-2625.

[10] Dubal, D. P., Ayyad, O., Ruiz, V., & Gomez-Romero, P. (2015). Hybrid energy storage: the merging of battery and supercapacitor chemistries. *Chemical Society Reviews*, *44*(7), 1777-1790.

[11] Rajesh, M., Manikandan, R., Park, S., Kim, B. C., Cho, W. J., Yu, K. H., & Raj, C. J. (2020). Pinecone biomass-derived activated carbon: the potential electrode material for the development of symmetric and asymmetric supercapacitors. *International Journal of Energy Research*, *44*(11), 8591-8605.

[12] Yin, J., Qi, L., & Wang, H. (2012). Sodium titanate nanotubes as negative electrode materials for sodium-ion capacitors. *ACS applied materials & interfaces*, *4*(5), 2762-2768.

[13] Li, B., Zheng, J., Zhang, H., Jin, L., Yang, D., Lv, H., & Zhang, C. (2018). Electrode materials, electrolytes, and challenges in nonaqueous lithium-ion capacitors. *Advanced Materials*, *30*(17), 1705670.

[14] Simon, P., & Gogotsi, Y. (2010). Materials for electrochemical capacitors. In *Nanoscience and technology: a collection of reviews from Nature journals* (pp. 320-329).

[15] Zhang, L., Hu, X., Wang, Z., Sun, F., & Dorrell, D. G. (2018). A review of supercapacitor modeling, estimation, and applications: A control/management perspective. *Renewable and Sustainable Energy Reviews*, *81*, 1868-1878.

[16] Zarzycki, P., Kerisit, S., & Rosso, K. M. (2010). Molecular dynamics study of the electrical double layer at silver chloride− electrolyte interfaces. *The Journal of Physical Chemistry C*, *114*(19), 8905-8916.

[17] Hunter, K. (2016). *Fundamental studies of electrochemical oxide formation on platinum single crystal electrodes* (Doctoral dissertation, Cardiff University).

[18] Vicentini, R., Da Silva, L. M., Franco, D. V., Nunes, W. G., Fiates, J., Doubek, G., ... & Zanin, H. (2021). Raman probing carbon & aqueous electrolytes interfaces and molecular dynamics simulations towards understanding electrochemical properties under polarization conditions in supercapacitors. *Journal of Energy Chemistry*, *60*, 279-292.

[19] Sinha, A., Jain, R., Zhao, H., Karolia, P., & Jadon, N. (2018). Voltammetric sensing based on the use of advanced carbonaceous nanomaterials: a review. *Microchimica Acta*, *185*(2), 1-30.

[20] Wei, L., & Yushin, G. (2012). Nanostructured activated carbons from natural precursors for electrical double layer capacitors. *Nano Energy*, *1*(4), 552-565.

[21] Simon, P., & Gogotsi, Y. (2013). Capacitive energy storage in nanostructured carbon–electrolyte systems. *Accounts of chemical research*, *46*(5), 1094-1103.

[22] Fernández, M., Valenciano, J., Trinidad, F., & Muñoz, N. (2010). The use of activated carbon and graphite for the development of lead-acid batteries for hybrid vehicle applications. *Journal of Power Sources*, *195*(14), 4458-4469.

[23] Lowke, J. J., & Morrow, R. (1995). Theoretical analysis of removal of oxides of sulphur and nitrogen in pulsed operation of electrostatic precipitators. *IEEE Transactions on Plasma Science*, *23*(4), 661-671.

[24] Han, W. Q. (2009). Anisotropic hexagonal boron nitride nanomaterials: synthesis and applications. *Nanotechnologies for the Life Sciences*.

[25] Chaitoglou, S. (2016). Growth Study and Characterization of Single Layer Graphene Structures Deposited on Copper Substrate by Chemical Vapor Deposition [Tesi].

[26] Guerrero-Contreras, J., & Caballero-Briones, F. (2015). Graphene oxide powders with different oxidation degree, prepared by synthesis variations of the Hummers method. *Materials Chemistry and Physics*, *153*, 209-220.

[27] Zhao, H., Ye, J., Song, W., Zhao, D., Kang, M., Shen, H., & Li, Z. (2020). Insights into the surface oxygen functional group-driven fast and stable sodium adsorption on carbon. *ACS Applied Materials & Interfaces*, *12*(6), 6991-7000.

[28] Shih, C. J., Lin, S., Sharma, R., Strano, M. S., & Blankschtein, D. (2012). Understanding the pH-dependent behavior of graphene oxide aqueous solutions: a comparative experimental and molecular dynamics simulation study. *Langmuir*, *28*(1), 235-241.

[29] Tang, C. (2017). *Exfoliation and restacking of manganese and cobalt based lamellar oxides for supercapacitor electrodes* (Doctoral dissertation, Université de Bordeaux).

[30] Li, Z., Wang, J., Liu, S., Liu, X., & Yang, S. (2011). Synthesis of hydrothermally reduced graphene/MnO2 composites and their electrochemical properties as supercapacitors. *Journal of Power Sources*, *196*(19), 8160-8165.

[31] Wu, C., Zhu, Y., Ding, M., Jia, C., & Zhang, K. (2018). Fabrication of plate-like MnO2 with excellent cycle stability for supercapacitor electrodes. *Electrochimica Acta*, *291*, 249-255.

[32] Zhang, K., Zhang, L. L., Zhao, X. S., & Wu, J. (2010). Graphene/polyaniline nanofiber composites as supercapacitor electrodes. *Chemistry of Materials*, *22*(4), 1392-1401.

[33] Lamiel, C., Tuma, D., & Shim, J. J. (2016). Non-aqueous synthesis of ultrasmall NiO nanoparticle-intercalated graphene composite as active electrode material for supercapacitors. *Materials Research Bulletin*, *83*, 275-283.

[34] Azwar, M. Y., Hussain, M. A., & Abdul-Wahab, A. K. (2014). Development of biohydrogen production by photobiological, fermentation and electrochemical processes: a review. *Renewable and Sustainable Energy Reviews*, *31*, 158-173.

[35] Tian, J., Zhao, Z., Kumar, A., Boughton, R. I., & Liu, H. (2014). Recent progress in design, synthesis, and applications of one-dimensional TiO 2 nanostructured surface heterostructures: a review. *Chemical Society Reviews*, *43*(20), 6920-6937.

[36] Kwade, A., Haselrieder, W., Leithoff, R., Modlinger, A., Dietrich, F., & Droeder, K. (2018). Current status and challenges for automotive battery production technologies. *Nature Energy*, *3*(4), 290-300.

[37] Mao, S., Pu, H., & Chen, J. (2012). Graphene oxide and its reduction: modeling and experimental progress. *Rsc Advances*, *2*(7), 2643-2662.

[38] Madito, M. J., Makgopa, K., Mtshali, C. B., & Bello, A. (2019). Graphene-Based Electrode Materials for Supercapacitor Applications. In *Electrochemical Devices for Energy Storage Applications* (pp. 101-130). CRC Press.

[39] Noori, A., El-Kady, M. F., Rahmanifar, M. S., Kaner, R. B., & Mousavi, M. F. (2019). Towards establishing standard performance metrics for batteries, supercapacitors and beyond. *Chemical Society Reviews*, *48*(5), 1272-1341.

[40] Yu, D., Goh, K., Wang, H., Wei, L., Jiang, W., Zhang, Q., ... & Chen, Y. (2014). Scalable synthesis of hierarchically structured carbon nanotube–graphene fibres for capacitive energy storage. *Nature nanotechnology*, *9*(7), 555-562.

[41] Tian, W., Gao, Q., Zhang, L., Yang, C., Li, Z., Tan, Y., ... & Zhang, H. (2016). Renewable graphene-like nitrogen-doped carbon nanosheets as supercapacitor electrodes with integrated high energy–power properties. *Journal of Materials Chemistry A*, *4*(22), 8690-8699.

[42] Hofmann, A., Migeot, M., Thißen, E., Schulz, M., Heinzmann, R., Indris, S., ... & Hanemann, T. (2015). Electrolyte Mixtures Based on Ethylene Carbonate and Dimethyl Sulfone for Li-Ion Batteries with Improved Safety Characteristics. *ChemSusChem*, *8*(11), 1892-1900.

[43] Afif, A., Rahman, S. M., Azad, A. T., Zaini, J., Islan, M. A., & Azad, A. K. (2019). Advanced materials and technologies for hybrid supercapacitors for energy storage–a review. *Journal of Energy Storage*, *25*, 100852.

[44] Kalinova, R., Dimitrov, I., Novakov, C., Veleva, S., & Stoyanova, A. (2021). Modular Platform for Synthesis of Poly (Ionic Liquid) Electrolytes for Electrochemical Applications in Supercapacitors. *ChemistrySelect*, *6*(15), 3795-3801.

[45] zwar, M. Y., Hussain, M. A., & Abdul-Wahab, A. K. (2014). Development of biohydrogen production by photobiological, fermentation and electrochemical processes: a review. *Renewable and Sustainable Energy Reviews*, *31*, 158-173

[46] Shakil, R., Shaikh, M. N., Shah, S. S., Reaz, A. H., Roy, C. K., Chowdhury, A. N., & Aziz, M. A. (2021). Development of a Novel Bio-based Redox Electrolyte using Pivalic Acid and Ascorbic Acid for the Activated Carbon-based Supercapacitor Fabrication. *Asian Journal of Organic Chemistry*, *10*(8), 2220-2230.

[47] Diederichsen, K. M., Fong, K. D., Terrell, R. C., Persson, K. A., & McCloskey, B. D. (2018). Investigation of solvent type and salt addition in high transference number nonaqueous polyelectrolyte solutions for lithium ion batteries. *Macromolecules*, *51*(21), 8761-8771.

[48] Wan, F., Zhu, J., Huang, S., & Niu, Z. (2020). High-voltage electrolytes for aqueous energy storage devices. *Batteries & Supercaps*, *3*(4), 323-330.

[49] Kato, Y., Kawamoto, K., Kanno, R., & Hirayama, M. (2012). Discharge performance of all-solid-state battery using a lithium superionic conductor Li10GeP2S12. *Electrochemistry*, *80*(10), 749-751.

[50] Vieira, D. F., Avellaneda, C. O., & Pawlicka, A. (2007). Conductivity study of a gelatin-based polymer electrolyte. *Electrochimica Acta*, *53*(4), 1404-1408.

[51] Dai, H., & Zawodzinski, T. A. (1998). The dependence of lithium transference numbers on temperature, salt concentration and anion type in poly (vinylidene fluoride)–hexafluoropropylene copolymer-based gel electrolytes. *Journal of Electroanalytical Chemistry*, *459*(1), 111-119.

[52] Anouti, M., Jacquemin, J., & Porion, P. (2012). Transport properties investigation of aqueous protic ionic liquid solutions through conductivity, viscosity, and NMR self-diffusion measurements. *The Journal of Physical Chemistry B*, *116*(14), 4228-4238.

[53] Aradilla, D., Estrany, F., & Aleman, C. (2011). Symmetric supercapacitors based on multilayers of conducting polymers. *The Journal of Physical Chemistry C*, *115*(16), 8430-8438.

[54] Mai, L., Li, H., Zhao, Y., Xu, L., Xu, X., Luo, Y., & Zhang, Q. (2013). Fast ionic diffusion-enabled nanoflake electrode by spontaneous electrochemical pre-intercalation for high-performance supercapacitor. *Scientific reports*, *3*(1), 1-8.

[55] Raza, W., Ali, F., Raza, N., Luo, Y., Kim, K. H., Yang, J., & Kwon, E. E. (2018). Recent advancements in supercapacitor technology. *Nano Energy*, *52*, 441-473.

[56] Täubert, C., Fleischhammer, M., Wohlfahrt-Mehrens, M., Wietelmann, U., & Buhrmester, T. (2010). LiBOB as electrolyte salt or additive for lithium-ion batteries based on LiNi0. 8Co0. 15Al0. 05O2/graphite. *Journal of The Electrochemical Society*, *157*(6), A721.

[57] Schütter, C., Pohlmann, S., & Balducci, A. (2019). Industrial requirements of materials for electrical double layer capacitors: impact on current and future applications. *Advanced Energy Materials*, *9*(25), 1900334.

[58] Ibrahim, T., Stroe, D., Kerekes, T., Sera, D., & Spataru, S. (2021, April). An overview of supercapacitors for integrated PV–energy storage panels. In *2021 IEEE 19th international power electronics and motion control conference (PEMC)* (pp. 828-835). IEEE.

[59] Wei, T., & Jia, D. (2014, June). Characteristics and design method of supercapacitor modules with voltage equalization circuit. In *2014 9th IEEE Conference on Industrial Electronics and Applications* (pp. 6-11). IEEE.

[60] MacFarlane, D. R., Tachikawa, N., Forsyth, M., Pringle, J. M., Howlett, P. C., Elliott, G. D., ... & Angell, C. A. (2014). Energy applications of ionic liquids. *Energy & Environmental Science*, *7*(1), 232-250.

[61] Zhao, X. Y., Yao, Z. T., & Li, J. H. (2010). Study on the properties and applications of molten salts. In *Proceedings of the 5th International Conference on Waste Management and Technology (ICWMT'10)* (Vol. 5, pp. 125-128).

[62] Serp, J., Allibert, M., Le Terrier, A., Malmbeck, R., Ougier, M., Rebizant, J., & Glatz, J. P. (2005). Electroseparation of actinides from lanthanides on solid aluminum electrode in LiCl-KCl eutectic melts. *Journal of The Electrochemical Society*, *152*(3), C167.

[63] Gorke, J., Srienc, F., & Kazlauskas, R. (2010). Toward advanced ionic liquids. Polar, enzyme-friendly solvents for biocatalysis. *Biotechnology and Bioprocess Engineering*, *15*(1), 40-53.

[64] Armand, M., Endres, F., MacFarlane, D. R., Ohno, H., & Scrosati, B. (2011). Ionic-liquid materials for the electrochemical challenges of the future. *Materials for sustainable energy: a collection of peer-reviewed research and review articles from Nature Publishing Group*, 129-137.

[65] Kadokawa, J. I. (2011). Preparation of polysaccharide-based materials compatibilized with ionic liquids. *Ionic Liquids: Applications and Perspectives*, 95-114.

[66] Alhanash, H. B. A. (2012). *Development of asymmetric ammonium-based room temperature ionic liquids*. The University of Manchester (United Kingdom).

[67] Tait, S., & Osteryoung, R. A. (1984). Infrared study of ambient-temperature chloroaluminates as a function of melt acidity. *Inorganic Chemistry*, *23*(25), 4352-4360.

[68] Vekariya, R. L. (2017). A review of ionic liquids: Applications towards catalytic organic transformations. *Journal of Molecular Liquids*, *227*, 44-60.

[69] Romero-Sanz, I., Bocanegra, R., Fernandez De La Mora, J., & Gamero-Castano, M. (2003). Source of heavy molecular ions based on Taylor cones of ionic liquids operating in the pure ion evaporation regime. *Journal of Applied Physics*, *94*(5), 3599-3605.

[70] Trost, B. M., & Czabaniuk, L. C. (2014). Structure and Reactivity of Late Transition Metal η3-Benzyl Complexes. *Angewandte Chemie International Edition*, *53*(11), 2826-2851.

[71] Gao, H., Shen, H., Wu, H., Jing, H., Sun, Y., Liu, B., ... & Hao, Q. (2021). Review of Pristine Metal–Organic Frameworks for Supercapacitors: Recent Progress and Perspectives. *Energy & Fuels*, *35*(16), 12884-12901.

[72] Asl, M. S., Hadi, R., Salehghadimi, L., Tabrizi, A. G., Farhoudian, S., Babapoor, A., & Pahlevani, M. (2022). Flexible all-solid-state supercapacitors with high capacitance, long cycle life, and wide operational potential window: Recent progress and future perspectives. *Journal of Energy Storage*, *50*, 104223.

[73] Yusuf, S. N. F., Yahya, R., & Arof, A. K. (2017). Ionic liquid enhancement of polymer electrolyte conductivity and their effects on the performance of electrochemical devices. *Progress and Developments in Ionic Liquids; Handy, S., Ed.; IntechOpen: London, UK*, 157-183.

[74] Latif, F. A., Zailani, N. A. M., Al Shukaili, Z. S. M., Zamri, S. F. M., Kasim, N. A. M., Rani, M. S. A., & Norrrahim, M. N. F. (2022). Review of poly (methyl methacrylate) based polymer electrolytes in solid-state supercapacitors. *Int. J. Electrochem. Sci*, *17*(22013), 2.

[75] Moreno-Fernández, G., Boulanger, N., Nordenström, A., Iakunkov, A., Talyzin, A., Carriazo, D., & Mysyk, R. (2021). Ball-milling-enhanced capacitive charge storage of activated graphene in aqueous, organic and ionic liquid electrolytes. *Electrochimica Acta*, *370*, 137738.

[76] Teran, F. D. E. (2016). *A new approach towards understanding the ion transfer dynamics in nanostructured carbon-based thin films for energy storage applications* (Doctoral dissertation, Université Pierre et Marie Curie-Paris VI).

[77] Liu, H., Maginn, E., Visser, A. E., Bridges, N. J., & Fox, E. B. (2012). Thermal and transport properties of six ionic liquids: an experimental and molecular dynamics study. *Industrial & Engineering Chemistry Research*, *51*(21), 7242-7254.

[78] Tokuda, H., Hayamizu, K., Ishii, K., Susan, M. A. B. H., & Watanabe, M. (2004). Physicochemical properties and structures of room temperature ionic liquids. 1. Variation of anionic species. *The Journal of Physical Chemistry B*, *108*(42), 16593-16600.

[79] Cao, Y., Chen, Y., Sun, X., Zhang, Z., & Mu, T. (2012). Water sorption in ionic liquids: kinetics, mechanisms and hydrophilicity. *Physical Chemistry Chemical Physics*, *14*(35), 12252-12262.

[80] Correia, D. M., Fernandes, L. C., Martins, P. M., García-Astrain, C., Costa, C. M., Reguera, J., & Lanceros-Méndez, S. (2020). Ionic liquid–polymer composites: A new platform for multifunctional applications. *Advanced Functional Materials*, *30*(24), 1909736.

[81] Pohlmann, S., Ramirez-Castro, C., & Balducci, A. (2015). The influence of conductive salt ion selection on EDLC electrolyte characteristics and carbon-electrolyte interaction. *Journal of the Electrochemical Society*, *162*(5), A5020.

Chapter-3

EXPERIMENTAL

3.1 Materials and Chemicals

In this study, analytical grade hydrochloric acid (HCl), potassium permanganate ($KMnO_4$), sodium nitrate ($NaNO_3$), polyvinylidene fluoride (PVDF), N-methyl-2-pyrrolidone (NMP), sulphuric acid (H_2SO_4), nitric acid (HNO_3), hydrogen peroxide (H_2O_2), 1-butyl-3-methyl-imidazolium chloride ($[Bmim]^+Cl^-$) were purchased from Merck, Germany and used without further purification. Neat $[Bmim]^+Cl^-$ was mixed with DI water to get different molar (0.1, 0.5, and 1.0 M) of $[Bmim]^+Cl^-$ electrolyte solutions. Deionized (DI) water was obtained using Barnstead Nanopore, Thermo Scientific, USA water purification system. All aqueous solutions of the experiments were prepared with DI water unless stated otherwise. 99.9% pure graphite plates were purchased from OTOOLWORLD, USA, and used as substrates to fabricate supercapacitor electrodes.

3.2 Synthesis of Graphene Oxide (GO) Using Improved Hammers' Method

The GO used in this experiment was produced using a two-step chemical oxidation procedure [1-5]. H_2SO_4 and HNO_3 (a ratio of 3:1) were combined in a 500 mL glass beaker and put in an oil bath at 80 ^oC while being vigorously magnetically stirred. 0.5 g of graphite flakes (1 wt%) were added to this solution after 3 minutes and maintained under constant stirring for 1.5 hours at 80 ^oC. The early oxidation of graphite is carried out via this process. Over the course of 30 minutes, the beaker was progressively filled with 3 g of $KMnO_4$ (2%) after which it was placed in an ice bath (0–5 ^oC). When the beaker was filled with the thick brown paste, it was moved to an oil bath at 45 oC and maintained under vigorous stirring for 1 hour, until it produced a thick brown paste. After that, the temperature was increased to 90 ^oC, and 50 mL of DI water was gently added to the solution while stirring continuously for 15 minutes. After that, the oil bath was withdrawn, and 50 mL of H_2O_2 was added to the solution in order to minimize the excess $KMnO_4$ in the solution. It is possible to create a brilliant yellow solution.

Aqueous solution of HCl was used to wash and filter the solution (37% HCl: DI water = 10:100 ml) many times, and then the solution was dialyzed in water to achieve neutral pH values in an aqueous environment. For 10 minutes, the solution was centrifuged at 4000 rpm in a centrifuge. The filtrate obtained after this process was dried in a vacuum oven at 40 ^{o}C for 24 hours to obtain GO.

3.3 Conversion of GO to rGO

The as-prepared GO was converted to rGO by a simple hydrothermal reaction [6-9]. In brief, 0.2 g of as-prepared GO was taken in a mixture of 50 ml of DI water a 10 ml of glycerin and sonicated for 2 hours. Then the GO suspension was taken into a stainless-steel autoclave and heated for the next 24 hours at 180 ^{o}C to get a gel-like product. After that, the product was washed several times with DI water and dried for 6 hours at 80 ^{o}C. The total synthesis procedure is shown in Figure 3.1.

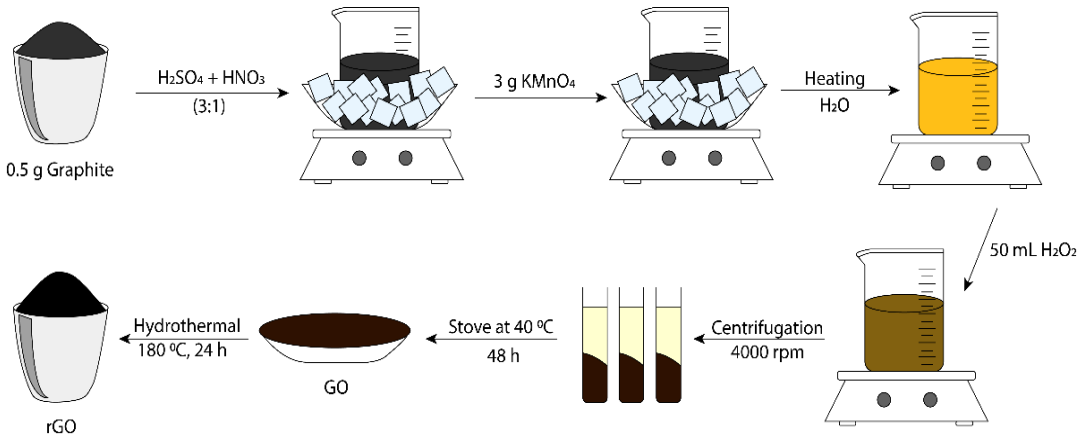

Figure 3.1. Synthesis scheme for the synthesis of GO by improved Hammers' method and conversion of GO to rGO

3.4 Morphological Characterization of Synthesized rGO Material

The phase purity levels and crystal structure of as-prepared GO and rGO were investigated using an X-ray diffractometer (XRD, Rigaku Ultima IV, Japan) with Cu-K-alpha radiation operated at a constant current of 40 mA and a constant voltage of 40 kV. The morphologies of the GO and rGO were visualized using a field emission scanning electron microscope (FESEM, TESCAN LYRA 3, Czech Republic). An Oxford Instruments Xmass detector equipped with the FESEM was used to carry out energy-dispersive X-ray spectroscopy (EDX). The Fourier transform infrared (FT-IR) spectra were recorded by an FT-IR spectrometer (Shimadzu) in the wave-number range (500-4000 cm^{-1}).

3.5 Electrochemical Evaluation of rGO electrode with ILs based Electrolytes

3.5.1 Cell Fabrication

The electrochemical properties of the as-obtained synthesized rGO were investigated under a two-electrode cell configuration [10-15] at 25°C in $[Bmim]^+Cl^-$ electrolytes diluted with water. The electrode materials (rGO) were firstly taken (10 mg) in a glass vial with 250 µL of NMP solution as a solvent, and PVDF as a binder. Then the glass vial was subjected to sonication for the next 30 minutes to get a slurry of active materials. About 20 µL (2 mg cm^{-2}) of the slurry was pasted on two polished disk-shaped graphite electrodes. Both the electrodes were dried under a hot air oven at 60 °C for 6 h to evaporate all the solvents. One of the electrodes was then put into the split coin cell and a separator made of Whatman filter paper (pore size, 11 µm) was placed right on this electrode material very gently. A few drops of freshly prepared diluted $[Bmim]^+Cl^-$ electrolytes were poured on the filter paper. When the filter paper seems completely wet, another electrode is placed upside down on this wet filter paper.

Finally, the cap of the split coin cell was assembled properly to complete the cell setup. A scheme of the cell setup is shown in Figure 3.2.

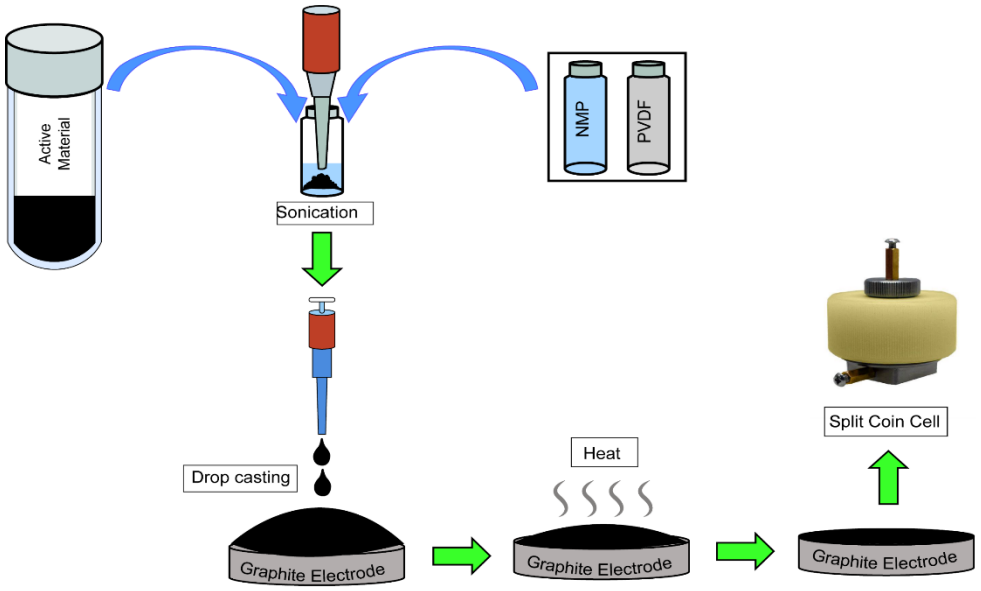

Figure 3.2. A schematic diagram for the cell setup.

3.5.2. Electrochemical measurement

Electrochemical investigations were accomplished with a computer-controlled electrochemical workstation (CHI 660E, USA) using a two-electrode system unless otherwise stated. Electrochemical properties of the fabricated supercapacitors were investigated using cyclic voltammetry (CV), galvanostatic charging-discharging (GCD), and electrochemical impedance spectroscopy (EIS) measurements. The analyses were carried out in $[Bmim]^+Cl^-$ electrolytes with three different concentrations within the potential range from 0 to 1.2 V unless otherwise stated. CV analyses were carried out at different scan rates from 10 to 200 mV s^{-1}. GCD analyses were performed at different current densities from 1 to 5 A g^{-1}. The cyclic stability test of the fabricated supercapacitor was conducted by repeating GCD cycles up to 10000 cycles at a fixed current density of 10 A g^{-1} within the same potential range of 0 to 1.2 V. The EIS was performed within the frequency range from 0.01 Hz to 1 MHz at an

AC amplitude of 10 mV in room temperature at the open circuit potential. The specific capacitance was calculated by using E_{qn} 3.1, as well as the energy and power density, were also calculated by using E_{qn} 3.2 and E_{qn} 3.3 respectively [16-18].

$$C_{sp}\ (Fg^{-1}) = \frac{2I\Delta t}{m\Delta V} \quad (3.1)$$

$$E\ (Whkg^{-1}) = \frac{C_{sp}.\Delta V^2}{8} \quad (3.2)$$

$$P\ (Wkg^{-1}) = \frac{E}{\Delta t} \quad (3.3)$$

$$\text{Capacitance retention} = \frac{n'th\ cycle\ capacitance}{1'st\ cycle\ capacitance} \times 100\ \% \quad (3.4)$$

$$\text{Coulombic efficiency, } \eta = \frac{t_{discharge}}{t_{charge}} \times 100\% \quad (3.5)$$

Where, I = applied current on the active material, Δt = Discharge time, m = Active mass on each electrode, ΔV = working potential window. The capacitance retention and the coulombic efficiency were calculated by using E_{qn} 3.4 and E_{qn} 3.5 respectively [16-18].

References

[1] Cui, C., Du, Y., Li, T., Zheng, X., Wang, X., Han, X., & Xu, P. (2012). Synthesis of electromagnetic functionalized Fe_3O_4 microspheres/polyaniline composites by two-step oxidative polymerization. *The Journal of Physical Chemistry B*, *116*(31), 9523-9531.

[2] Marcano, D. C., Kosynkin, D. V., Berlin, J. M., Sinitskii, A., Sun, Z., Slesarev, A., & Tour, J. M. (2010). Improved synthesis of graphene oxide. *ACS nano*, *4*(8), 4806-4814.

[3] Chen, J., Yao, B., Li, C., & Shi, G. (2013). An improved Hummers method for eco-friendly synthesis of graphene oxide. *Carbon*, *64*, 225-229.

[4] Liu, H., Dong, X., Wang, X., Sun, C., Li, J., & Zhu, Z. (2013). A green and direct synthesis of graphene oxide encapsulated TiO_2 core/shell structures with enhanced photoactivity. *Chemical engineering journal*, *230*, 279-285

[5] Wang, C., Lan, Y., Yu, W., Li, X., Qian, Y., & Liu, H. (2016). Preparation of amino-functionalized graphene oxide/polyimide composite films with improved mechanical, thermal and hydrophobic properties. *Applied Surface Science*, *362*, 11-19.

[6] Kaur, G., Kumar, R., & Lahiri, I. (2019). Field electron emission from protruded GO and rGO sheets on CuO and Cu nanorods. *Physica E: Low-dimensional Systems and Nanostructures*, *112*, 10-18.

[7] Tan, Q., Kong, Z., Guan, X., Zhang, L. Y., Jiao, Z., Chen, H. C., ... & Xu, B. (2019). Hierarchical zinc oxide/reduced graphene oxide composite: preparation route, mechanism study and lithium-ion storage. *Journal of colloid and interface science*, *548*, 233-243.

[8] Liao, J., Ye, M., Han, A., Guo, J., Liu, Q., & Yu, G. (2021). Boosted electromagnetic wave absorption performance from multiple loss mechanisms in flower-like Cu_9S_5/RGO composites. *Carbon*, *177*, 115-127.

[9] Sengupta, D., Ghosh, S., & Basu, B. (2017). Advances and Prospects of Graphene Oxide (GO) as Heterogeneous' Carbocatalyst'. *Current Organic Chemistry*, *21*(9), 834-854.

[10] Chen, H., Hu, L., Yan, Y., Che, R., Chen, M., & Wu, L. (2013). One-step fabrication of ultrathin porous nickel hydroxide-manganese dioxide hybrid nanosheets for supercapacitor electrodes with excellent capacitive performance. *Advanced Energy Materials*, *3*(12), 1636-1646.

[11] De Adhikari, A., Morag, A., Seo, J., Kim, J. M., & Jelinek, R. (2020). Polydiacetylene–perylenediimide supercapacitors. *ChemSusChem*, *13*(12), 3230-3236.

[12] Kumar, N., Huang, C. W., Yen, P. J., Wu, W. W., Wei, K. H., & Tseng, T. Y. (2016). Probing the electrochemical properties of an electrophoretically deposited Co_3O_4/rGO/CNTs nanocomposite for supercapacitor applications. *RSC advances*, *6*(65), 60578-60586.

[13] Tabrizi, A. G., Arsalani, N., Mohammadi, A., Namazi, H., Ghadimi, L. S., & Ahadzadeh, I. (2017). Facile synthesis of a Mn_2Fe_4/rGO nanocomposite for an ultra-stable symmetric supercapacitor. *New Journal of Chemistry*, *41*(12), 4974-4984.

[14] Xiong, C., Li, T., Zhu, Y., Zhao, T., Dang, A., Li, H., & Khan, M. (2017). Two-step approach of fabrication of interconnected nanoporous 3D reduced graphene oxide-carbon nanotube-polyaniline hybrid as a binder-free supercapacitor electrode. *Journal of Alloys and Compounds*, *695*, 1248-1259.

[15] Xu, K., Zou, R., Li, W., Liu, Q., Liu, X., An, L., & Hu, J. (2014). Design and synthesis of 3D interconnected mesoporous $NiCo_2O_4$@ $Co_xNi_{1-x}(OH)_2$ core–shell nanosheet arrays with large areal capacitance and high-rate performance for supercapacitors. *Journal of Materials Chemistry A*, *2*(26), 10090-10097.

[16] Aghazadeh, M., Dalvand, S., & Hosseinifard, M. (2014). Facile electrochemical synthesis of uniform β-$Co(OH)_2$ nanoplates for high performance supercapacitors. *Ceramics International*, *40*(2), 3485-3493.

[17] Wang, J. G., Yang, Y., Huang, Z. H., & Kang, F. (2013). Effect of temperature on the pseudo-capacitive behavior of freestanding MnO_2@ carbon nanofibers composites electrodes in mild electrolyte. *Journal of Power Sources*, *224*, 86-92.

[18] Tang, Y., Liu, Y., Yu, S., Mu, S., Xiao, S., Zhao, Y., & Gao, F. (2014). Morphology controlled synthesis of monodisperse cobalt hydroxide for supercapacitor with high performance and long cycle life. *Journal of Power Sources*, *256*, 160-169.

Chapter-4

RESULTS AND DISCUSSION

4.1 Characterization

4.1.1 Functional Group Identification of GO and rGO by FTIR

FTIR was used in order to investigate the presence of functional groups in the samples from the obtained vibrational (transmittance/absorption) spectra. This analysis is based on the vibrational excitation of molecular bonds by absorption of infrared light energy, within the wavelength from 4000 to 400 cm^{-1}. GO, the oxide form of graphite is expected to contain more oxygen-containing functional groups after the oxidation process. However, with reduction, rGO is expected to have a minimal amount of oxygen-containing functional groups. The FTIR spectra of the GO and rGO samples are shown in Figure 4.1. For GO an intense and broad peak appeared at a wavelength of 3420 cm^{-1} confirming the presence of O-H bond (hydroxyl group). Besides, –C=O stretching (–COOH group) was presented at 1739 cm^{-1} whereas C-O-C stretching (epoxy group) can be seen at a wavelength of 1226 and 1015 cm^{-1} [1]. With the presence of all these carboxylic, hydroxyl, epoxide, and carbonyl groups, oxygen molecules (O) were confirmed to be greatly occupied at the edge and basal plane of GO which can be concluded that GO was synthesized successfully [2]. The FTIR characteristic peak and corresponding interpretations for GO and rGO are shown in Table 4.1.

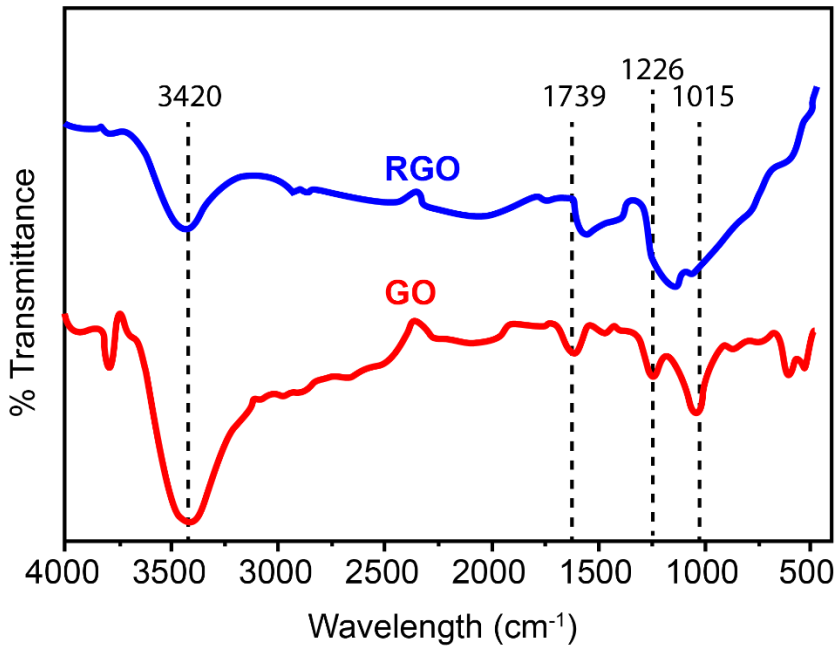

Figure 4.1. FTIR spectra for GO and rGO

For rGO, the peak at 3420 cm^{-1} became less broad as compared with GO proving that the hydroxyl group was removed significantly [3]. It is also noticeable that other peaks at 1739, 1226, and 1015 cm^{-1} became less intense than those peaks at the same location in FTIR spectra of GO, which were also due to the hydrothermal treatment at 180 ^{o}C. Therefore, the oxygen-containing functional groups were successfully removed partially and the low amounts of the residue of functional groups remain at the edge and basal plane of rGO.

Table 4.1. FTIR characteristic peak and corresponding interpretations for GO and rGO

Wavenumber (cm^{-1})	Interpretations
3420	–OH stretching
1739	C=O (COOH) stretching
1226	C-O-C stretching
1015	C-O-C stretching

4.1.2 Structural Analysis of GO and rGO by XRD

The XRD analysis of synthesized GO, and rGO samples allowed to see how the interlayer distances, a key measure of structural change, varied among the samples as well to determine their crystallinity and phase purity. For comparison, the corresponding data about RGO and GO were also given in Figure 4.2. Generally, a sharp peak can be observed at $2\theta = 26.62°$ for pure graphite [4]. This peak confirmed the presence of a well-arranged layer structure with 0.3346 nm d-spacing, along with the (002) orientation [4]. In Figure 2, the 2θ peak for GO can be seen to be shifted to 9.03°, which indicated that the graphite was fully oxidized into GO. Furthermore, the interlayer distance of GO was increased with a d-spacing of 0.9794 nm (FWHM = 0.6298). This increment resulted from the intercalation of oxide functional groups at the carbon basal plane such as epoxy, hydroxyl, carbonyl, and carboxyl groups during the chemical oxidation reaction. Therefore, the distance between consecutive carbon layers increased.

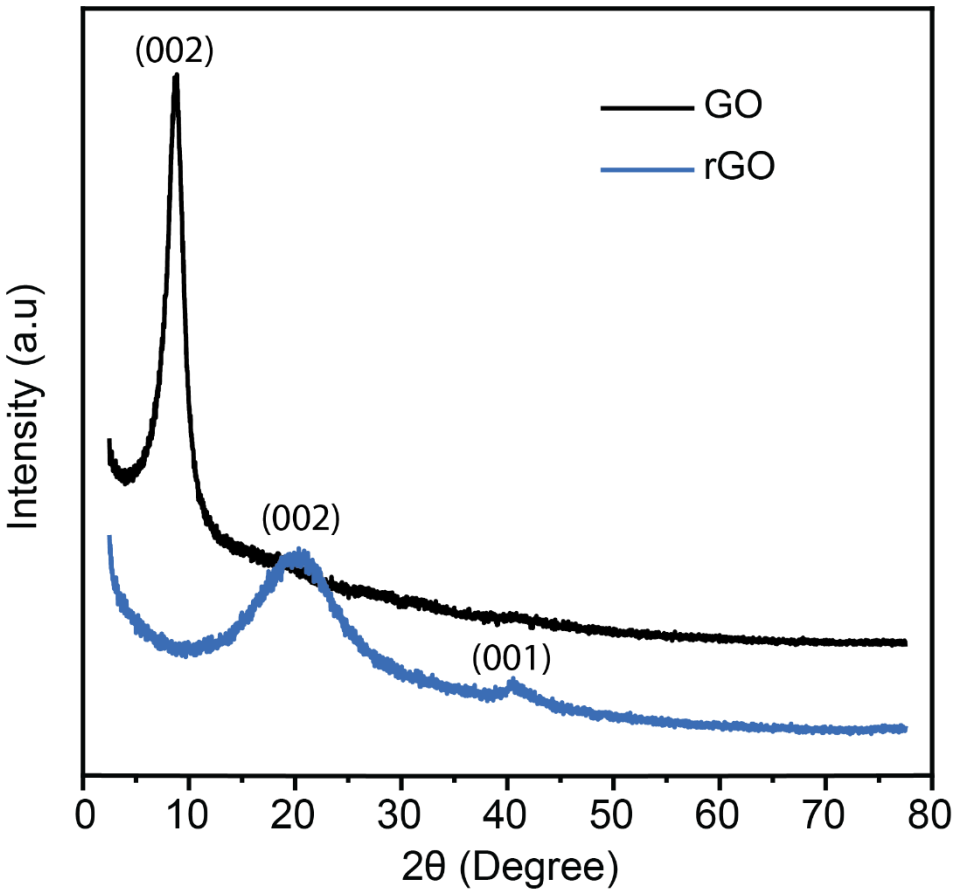

Figure 4.2. XRD spectra of GO and rGO

After oxygen-containing functional groups were eliminated significantly during the hydrothermal reduction, a broader peak can be seen for rGO at 2θ = 24.10°. This indicates that the π-conjugated structure of graphene has been restored considerably at the produced rGO [5]. The presence of a broad peak (002) for rGO implied that the crystal phase (002) was arranged randomly as compared to the high crystallization structure of graphite where a sharp and intense (002) peak can be observed (Figure 2) [6]. The poor arrangement could be caused by the formation of a single or only a few layers of rGO after being reduced from GO. In addition, the d-spacing of rGO was reduced from 0.97942 nm to 0.36895 nm which proved that oxygen-containing functional groups were removed efficiently. It also revealed that the thin rGO nanosheet was stacked to each other to form thick piles structure due to the existence of strong Van der Waals forces between each layer. Another less intense peak can be seen at 2θ=42.60° with (001) orientation which is attributed to the turbostratic band of disordered carbon materials [7].

4.1.3 Surface Morphology and Elemental Analysis by FESEM and EDX

The surface morphology of the synthesized samples was studied through Field Emission Scanning Electron Microscopy (FESEM). This Characterization gives the optical specifications of the entire or fractioned surfaces as per needed [8]. It lays down the topographical and elemental particulars with higher magnifications and provides a much more lucid picture of the samples. The morphological analysis of GO and rGO was carried out from FESEM images to observe the difference in the characteristics of these materials in terms of particle shape, particle distribution, and surface morphology. Figure 4.3 and 4.4 show FESEM images of the GO as well as hydrothermally reduced rGO respectively synthesized by improved Hummer's method.

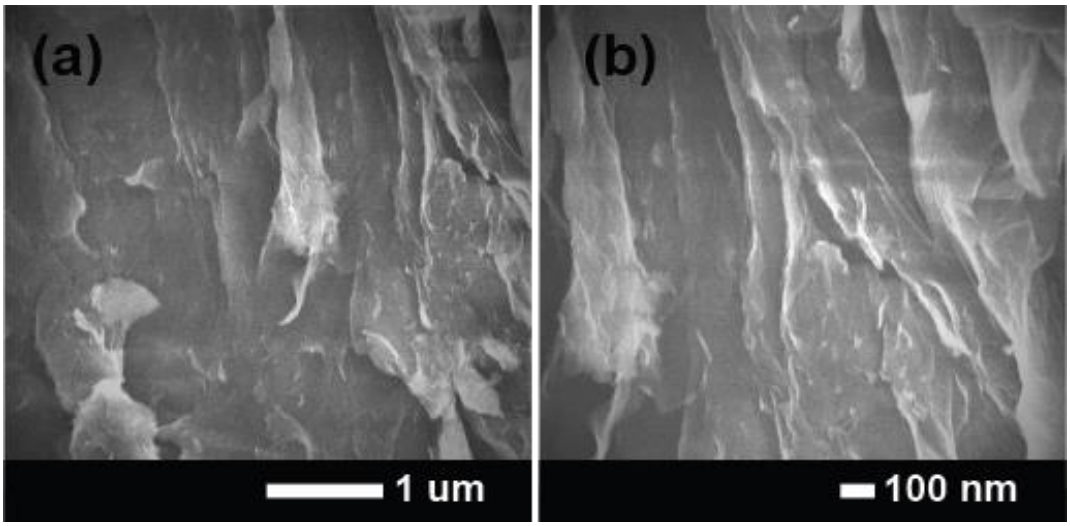

Figure 4.3. FESEM images of the GO

For GO, the synthesis process used governs the micro surface-level details. The synthesized GO exhibited a much defined, flaky, layered, 2-dimensional, fold-like microstructure with a heavy wrinkled effect to it as shown in Figure 4.3 (a). Such structure is possibly due to deformation caused by the exfoliation and restacking during the synthesis process. There are certain defects associated with the surfaces; partially due to sizeable numbers of functional groups: –OH and –COOH attached to the edge and –C–O–C and –COOH groups in the internal areas. The interlayered length of the graphitic sheets swells due to these functional groups and thus dismantles the integrated layered microstructure leading to a wrinkled surface appearance [9]. Along with the stacked layer, the FESEM images in Figure 4.3 (b) also indicate a big sheet of GO was

obtained beyond the whole observation region, which is good for the reduction experiments.

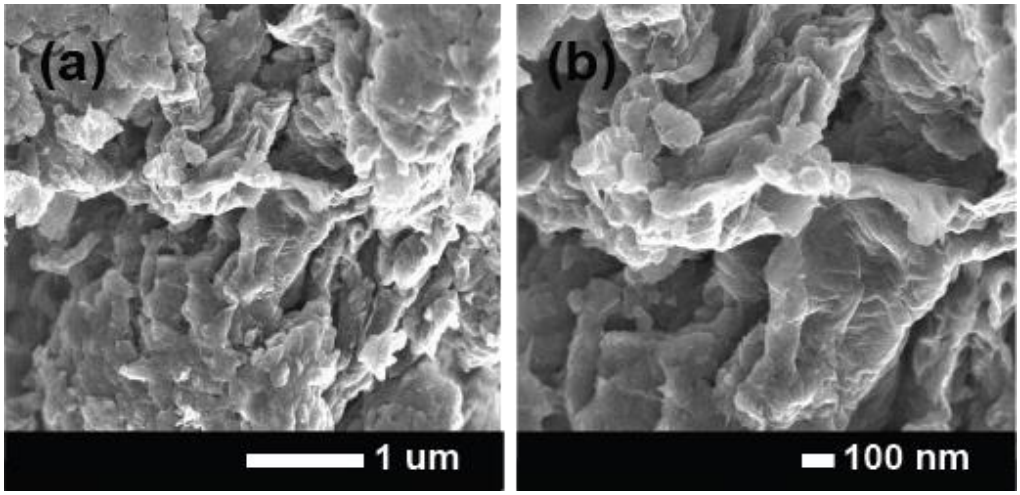

Figure 4.4. (a), and (b) represents the FESEM images of hydrothermally reduced rGO

After reduction, big GO sheets are starting to tilt slowly, namely, the layers start stripping and become layered structures. Figure 4.4 (a) and (b) show the micrograph of the as prepared rGO. An apparent layered construction was being seen for rGO, giving out a wrinkled effect, like GO. The rGO surface contained crumpled thin sheets which accumulated to form disordered structure material. The FESEM images of rGO (Figure 4.4 (b)) also demonstrate thin and wrinkled sheets, forming a cabbage-like structure. The decrease in the thickness of the rGO nanosheets is due to several factors, including the removal of oxygen-containing functional groups by heating and elimination of the interlamellar water present in GO [10]. However, the stacking of the rGO sheets is much looser and there are larger gaps in between the stacks. This suggests that rGO could allow more electrolyte ion adsorption during the charging-discharging process.

The energy-dispersive X-ray (EDX) spectrum of GO and rGO is shown in Figure 4.5. The EDX analysis revealed that the composition of GO sheets mostly consisted of C and O (70 wt% C and 30 wt% O) (Figure 4.5) and show quite good or almost similar results as compared to reported Hummers or modified Hummer's method in which a mixture of HNO_3 and $NaNO_3$ was utilized as an oxidizing agent. These analytical results prove the good oxidizing efficiency of our protocol since we have not used $NaNO_3$ during the oxidation of graphite flakes. From the EDX spectrum of rGO (Figure

4.5), the decreased oxygen content (81 wt% C and 19 wt% O) proves the successful reduction of GO into rGO.

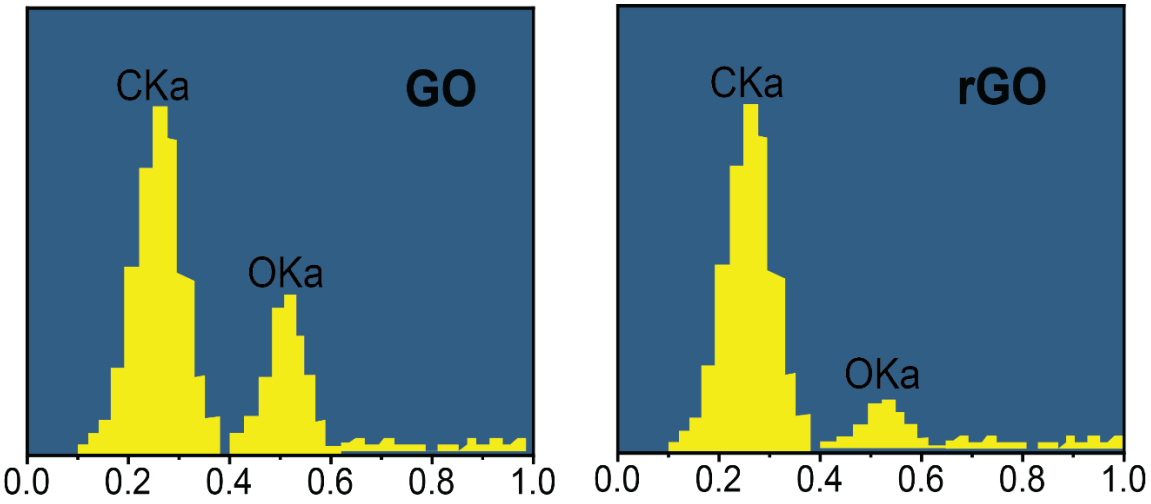

Figure 4.5. EDX spectroscopy of GO and rGO

4.2 Electrochemical Performance Analysis

The electrochemical tests were first conducted in two-electrode Swagelok cells using pure $[Bmim]^+Cl^-$ and $[Bmim]^+Cl^-/H_2O$ electrolytes with different concentrations from 0.1 to 1.0 M and using the same upper cutoff potentials of 2.4 V at room temperature. The positive and negative electrodes were loaded with equal amounts of active materials. For clarity, the current densities and all specific charge storage capabilities reported are based on the total mass of active materials in a cell.

4.2.1 Electrochemical Evaluation of rGO Electrode in Pure $[Bmim]^+Cl^-$ Electrolyte

Figure 4.6 (a) represents CVs of the rGO-based supercapacitor in pure $[Bmim]^+Cl^-$ electrolyte at different scan rates (10-200 mV s^{-1}). The CV curve of the as-prepared rGO with pure $[Bmim]^+Cl^-$ electrolytes shows an ideal rectangular shape from 0 to 2.4 V, indicating good capacitive behavior for charging the electrical double layer. The motion of the $[Bmim]^+$ and its counterion Cl^- is responsible for the formation/dissociation of the double layers [11]. The rectangularity of the CVs is

retained within the operating potential window even at a high scan rate of 200 mV s^{-1} indicating a good diffusion of electrolytes ions at the electrode-electrolyte interface [12]. The GCD curves of the rGO-based supercapacitor in pure $[Bmim]^+Cl^-$ at different current densities from 0.5-5 A g^{-1} within 2.4 V are shown in Figure 4.6 (b). It was observed that the current density has a significant impact on the charge storage ability. Both the charge and discharge time decreased with the increase in current density, indicating a decrease in the capacity of charge storage. The potential *vs* time curves showed symmetrical triangular shapes at all current densities. The C_{sp} values for the rGO-based supercapacitor in pure $[BMIM]^+Cl^-$ electrolyte are 104, 100, 83, 62, and 41 F g^{-1} at the current density of 0.5, 1, 2, 3, and 5 A g^{-1} respectively.

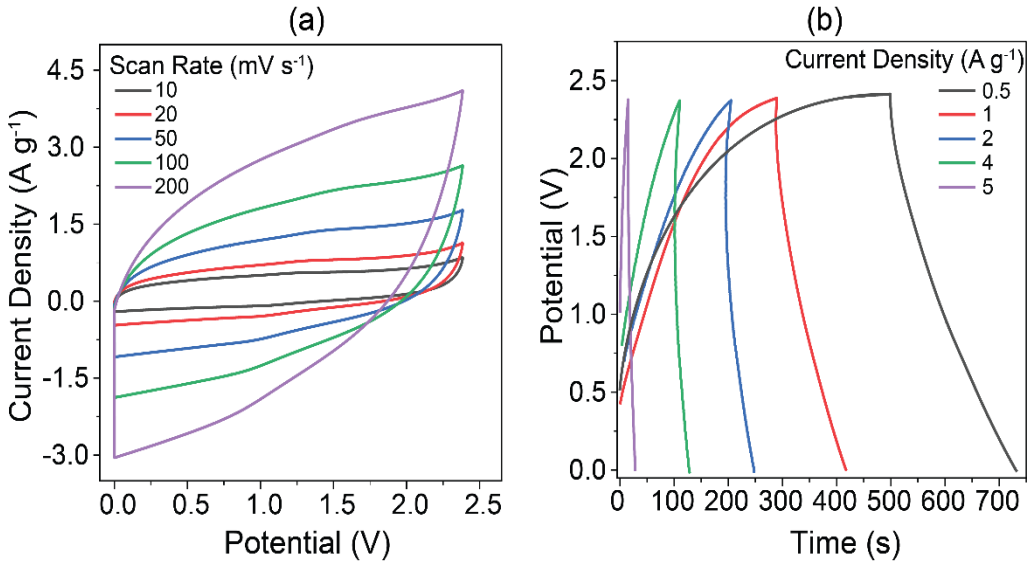

Figure 4.6. (a) represents the CVs of rGO in pure $[Bmim]^+Cl^-$ electrolyte, and (b) represents the GCD curves of rGO in pure $[Bmim]^+Cl^-$ electrolyte.

However, a rather slow discharge process was observed at the beginning of each discharge after an appreciable IR drop. The internal resistance value was calculated as 9 ohms from the IR drop, which is slightly higher than that of supercapacitors with aqueous (e.g., aqueous H_2SO_4 or KOH) or organic (e.g., TEA/BF_4 in acetonitrile or propylene carbonate) electrolytes [13, 14]. This slow charge-discharge process and high internal resistance most likely arise from the lower conductivity value of the $[Bmim]^+Cl^-$ electrolyte and higher viscosity, as compared to aqueous or organic electrolytes [15]. Current work on water dilution of $[Bmim]^+Cl^-$ electrolyte for higher ion conductivity is underway in an effort to address these issues.

4.2.2 Comparative Study with Different ILs-Based Electrolyte

To check the dilution effect of $[Bmim]^+Cl^-$ with water as SC electrolyte, the CV, GCD has furtherly done for rGO-based SC with 0.5 M of $[Bmim]^+Cl^-/H_2O$ electrolyte. The comparative CV curve of rGO with pure $[Bmim]^+Cl^-$ and 0.5 M $[Bmim]^+Cl^-/H_2O$ electrolyte is shown in Figure 4.7 (a). The CV curves were close to being rectangular in shape at the scan rate of 20 mV s^{-1}, which is typical capacitive behavior for graphene-based supercapacitors [16]. Although the presence of the functional groups on the surface of the rGO sheets likely contributed to a small amount of pseudocapacitance, the linearity of the measured current indicates that our devices are primarily non-faradaic within the voltage of 2.4 V. Interestingly, in 0.5 M $[Bmim]^+Cl^-/H_2O$ electrolyte, the capacitive response of the rGO-based SC is better than the pure $[Bmim]^+Cl^-$ electrolyte. The area under the CV curve of EDLCs in 0.5 M $[Bmim]^+Cl^-/H_2O$ is higher than in the pure $[Bmim]^+Cl^-$ electrolyte system. This confirmed the enhanced capacitive performance of rGO in 0.5 M $[Bmim]^+Cl^-/H_2O$. Both the anodic and cathodic current rise of rGO in 0.5 M $[Bmim]^+Cl^-/H_2O$ is more controlled at a high potential region than the pure $[Bmim]^+Cl^-$ electrolytic system. It also indicates the homogeneous distribution of ionic charges of 0.5 M $[Bmim]^+Cl^-/H_2O$ over the surface of rGO electrodes at the potential of 2.4 V [17].

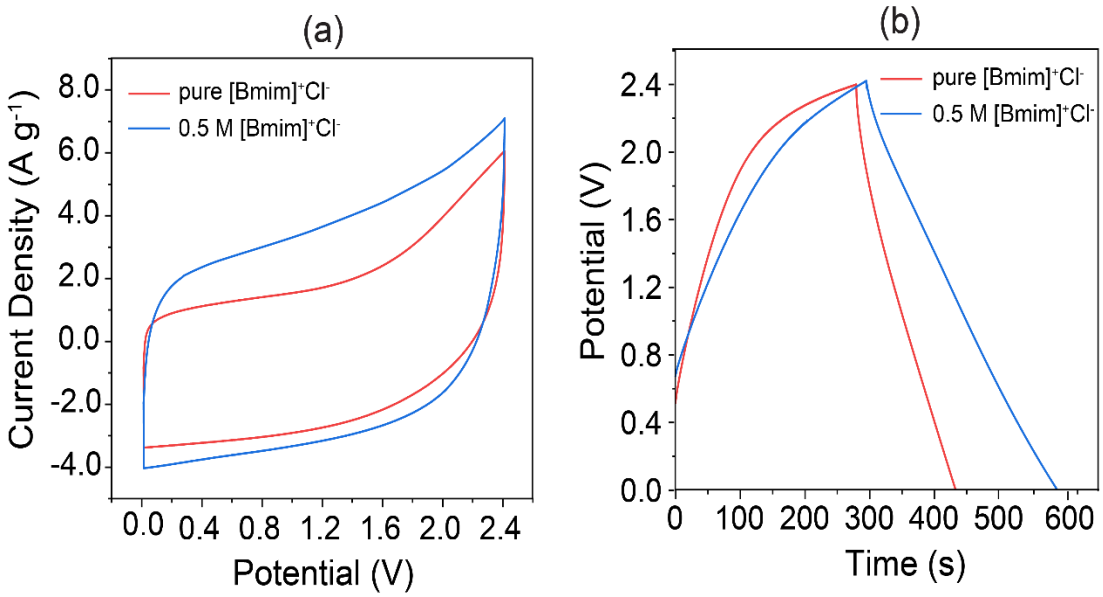

Figure 4.7. (a) represents the comparative CVs of rGO in pure and diluted $[Bmim]^+Cl^-$ electrolyte, and (b) represents the GCD curves of rGO in pure and diluted $[Bmim]^+Cl^-$ electrolyte.

The charge storage performance of the rGO was further investigated using GCD with $[Bmim]^+Cl^-/H_2O$ and pure $[Bmim]^+Cl^-$ electrolytes in a symmetrical two-electrode system. Figure 4.7 (b) shows the typical comparison of the GCD curves (at a fixed current density of 1 Ag^{-1}) of the rGO in the two different electrolytic systems. Pseudo-symmetric triangular shapes, *i.e.*, unequal charging-discharging time, appeared for all the electrolytes. It suggests that the rGO exhibits good reversibility in all the electrolytes [18]. However, the highest discharging time was also obtained in 0.5 M $[Bmim]^+Cl^-/H_2O$. It supports the highest level of EDLC formation for the rGO electrode in 0.5 M $[Bmim]^+Cl^-/H_2O$. The absence of IR-drop in the GCD curves, due to the easy accessibility of electrolyte ions into the layered and porous structure of the electrode material, demonstrates the fabricated supercapacitors' high conductivity in the diluted $[Bmim]^+Cl^-/H_2O$ electrolytes. However, the Pure $[Bmim]^+Cl^-$ electrolyte showed lower specific capacitance than the diluted $[Bmim]^+Cl^-/H_2O$ electrolytes, suggesting the possible influence of the varied electrolyte viscosity on the transport properties [19]. Furthermore, the high capacitive response with diluted 0.5 M $[Bmim]^+Cl^-/H_2O$ electrolyte indicating more inner surface areas of the rGO electrode materials were utilized for charge storage. The total electrochemical performance of the rGO electrode in 0.5 M $[Bmim]^+/H_2O$ electrolyte is shown in Table 4.2.

Table 4.2. The total electrochemical performance of rGO in 0.5 M $[Bmim]^+/H_2O$ electrolyte.

	Current Density ($A\ g^{-1}$)	C_{sp} ($F\ g^{-1}$)	E ($Wh\ kg^{-1}$)	P ($W\ kg^{-1}$)
0.5 M $[Bmim]^+/H_2O$	1	234	47	600
	2	167	34	1200
	3	112	23	1800
	5	104	20	3000

To fix the electrochemical potential window of 0.5 M $[Bmim]^+Cl^-/H_2O$ electrolyte, CV was performed (Figure 4.8 (a)) in different potential window ranges from 0-2.0 V to 0-

2.8 V at a fixed scan rate of 20 mV s^{-1}. It was observed that the area under the CV curve increases with the enhancement of the potential window to 2.4 V. Beyond 2.4 V the electrolyte solution started to decompose as the CV shapes shown in Figure 4.8 (a) at 2.6 and 2.8 V is upward trending. The electrochemical stable window was finally determined by performing GCD within the similar potential windows as CVs at a fixed current density of 1 A g^{-1} shown in Figure 4.8 (b). With the increase in the potential window from 0-2.0 V to 0-2.4 V, the specific capacitance also increased, and the highest capacitance was found 234 F g^{-1} within the window of 0-2.4 V. At 0-2.6 V and 0-2.8 V, a small IR drop was observed which resulted in the decrease in supercapacitor performance.

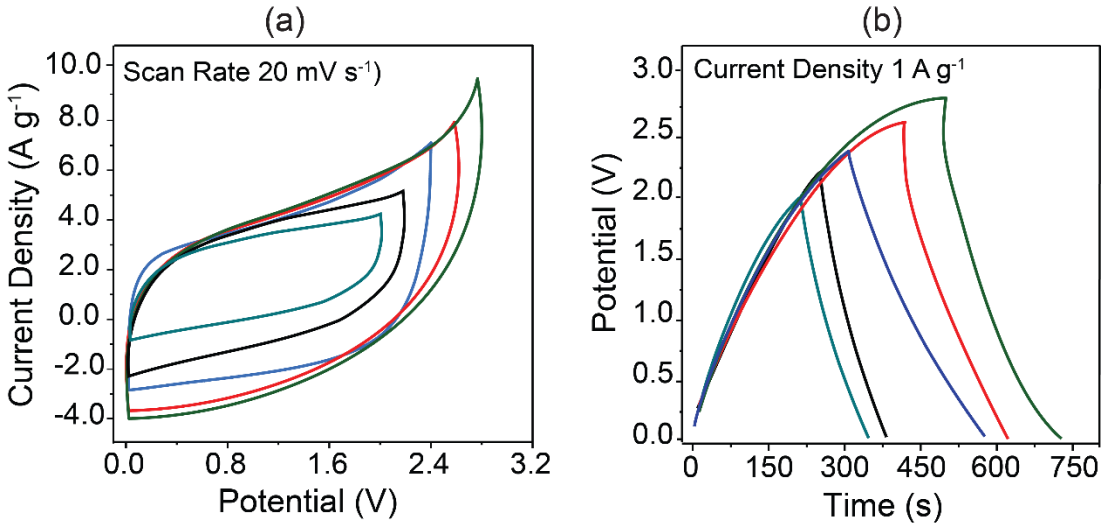

Figure 4.8. (a) Comparative CV for 0.5 M $[Bmim]^+Cl^-/H_2O$ electrolyte in different window at 20 mV s^{-1}. (b) Comparative GCD for 0.5 M $[Bmim]^+Cl^-/H_2O$ electrolyte in different window at 1 A g^{-1}.

Interestingly, by limiting the O_2/H_2 evaluation, the 0.5 M $[Bmim]^+Cl^-/H_2O$ electrolyte can broaden the thermodynamic stability of water [20]. Generally, the acid equilibrium of water and the hydrogen bond between the hydrogen molecule to its nearest oxygen molecule in the water are the two major factors that are responsible for water decomposition. Since $[Bmim]^+Cl^-$ is highly soluble in water, strong hydration of $[Bmim]^+$ and Cl^- with water may result in lowering the free water content to be attached to H^+ to form H_3O^+ ion [21]. Note that lowering the hydrogen bond causes a strong O-H bond which results in this wide potential window. Thus, by using diluted $[Bmim]^+Cl^-$ electrolyte the electrochemical window of rGO-based supercapacitors is enhanced.

Now, to gain insight into the role of dilution on the capacitance of the rGO electrode, CV and GCD has been furtherly done by varying the electrolyte concentration of 0.1, 0.5, and 1 M $[Bmim]^+Cl^-/H_2O$ electrolyte. Figure 4.9 illustrates the influence of the concentration of the $[Bmim]^+Cl^-/H_2O$ electrolytes at a fixed potential of 2.4 V. However, it has been shown that 0.5 M $[Bmim]^+Cl^-/H_2O$ showed better conductivity as a better current response shown in the CV, GCD curve (Figure 4.9 (a, b)) than 1.0 M and 0.1 M $[Bmim]^+Cl^-/H_2O$ electrolyte solutions. This phenomenon can be explained by the association of $[Bmim]^+Cl^-$ ions which are responsible for less water hydration at 1.0 M $[Bmim]^+Cl^-/H_2O$ concentration [22]. Whereas, at 0.1 M concentration, the insufficient electrolyte ions mobility inhibits the rapid charging/discharging process due to the decrease in ionic mobility [22]. So, the 0.5 M $[Bmim]^+Cl^-/H_2O$ requires low activation energy and can be considered as optimum electrolyte concentration for the PC-based supercapacitor.

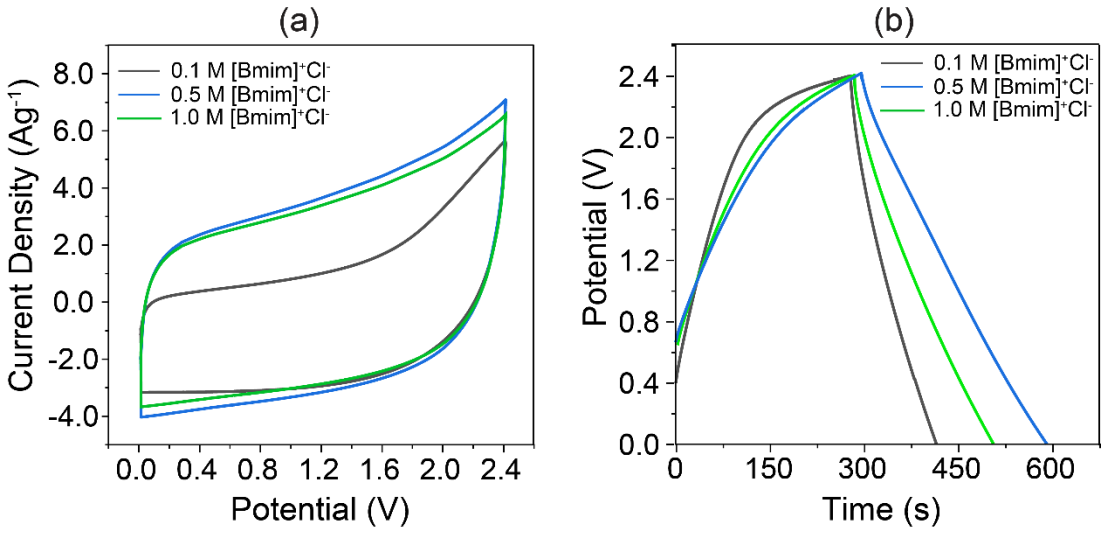

Figure 4.9. (a) CV of rGO at different $[Bmim]^+Cl^-/H_2O$ electrolyte concentrations at 20 mV s^{-1}, (b) GCD of rGO at different $[Bmim]^+Cl^-/H_2O$ electrolyte concentrations at 1 A g^{-1}.

The Ragone plot of the studied electrolytes is shown in Figure 4.10. The pure $[Bmim]^+Cl^-$ electrolyte show enhanced energy densities but relatively poor rate capabilities. The conductivity of $[Bmim]^+Cl^-$ increases with the water dilution as a result of increased Coulombic interactions of the ionic species. It has been overviewed that most aqueous electrolytes with carbon-based electrodes have a maximum energy density of about 30-70 Wh kg^{-1} [23]. Remarkably, a maximum energy density of 47

Wh kg^{-1} with a power density of 600 W kg^{-1} was observed for the 0.5 M $[Bmim]^+Cl^-/H_2O$ electrolyte in this work. They are much higher than those of a previously reported aqueous electrolyte and also higher than those with ionic liquid in acetonitrile as electrolyte and rGO as electrodes. Such a high energy density of the present electrolytes is associated with the optimum concentration of the electrolyte ions, high ion conductivity, and high operating voltage. The total performance of the four electrolytic systems is shown in Table 4.3.

Table 4.3. The total performance of the rGO electrode with the four different electrolytic systems.

Electrolytic System	Current Density ($A\ g^{-1}$)	C_{sp} ($F\ g^{-1}$)	E ($Wh\ kg^{-1}$)	P ($W\ kg^{-1}$)	R_s (ohm)
Pure $[Bmim]^+Cl^-$	1.0	100.00	20.00	600.00	22
	2.0	83.33	16.67	1200.00	
	3.0	62.50	12.50	1800.00	
	5.0	41.67	8.33	3000.00	
0.1 M $[Bmim]^+Cl^-$	1.0	83.33	16.67	600.00	12
	2.0	63.33	12.67	1200.00	
	3.0	50.00	10.00	1800.00	
	5.0	37.50	7.50	3000.00	
0.5 M $[Bmim]^+Cl^-$	1.0	233.33	46.67	600.00	8
	2.0	166.67	33.33	1200.00	
	3.0	112.50	22.50	1800.00	
	5.0	104.17	20.83	3000.00	
1.0 M $[Bmim]^+Cl^-$	1.0	175	35	600.00	10
	2.0	150	30	1200.00	
	3.0	100	20	1800.00	
	5.0	83.33	16.67	3000.00	

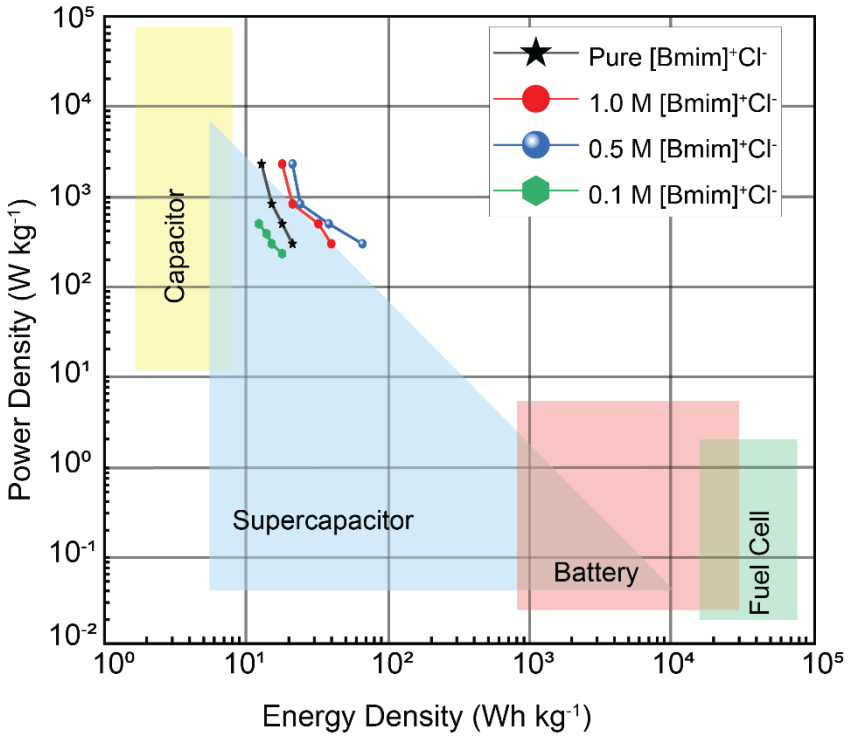

Figure 4.10. Ragoon plot

4.2.3 EIS and Cyclic Stability Test of rGO with Pure and Diluted $[Bmim]^+Cl^-$ electrolyte

To further evaluate the device performance, the frequency response of the supercapacitor incorporating the rGO electrodes with pure and diluted $[Bmim]^+Cl^-$ electrolyte was analyzed using electrical impedance spectroscopy (EIS). Figure 4.11 (a) shows the Nyquist plot in the frequency range of 0.05 Hz to 1 MHz, with the lower-left portion of the curve corresponding to the higher frequency. The depressed semicircle in the high-frequency region is modeled by a parallel combination of an interfacial charge transfer resistance and the double-layer capacitance [24]. The inclined portion of the curve spanning real resistances (Z') of approximately 8.0 to 22.0 is typically represented by the Warburg impedance that pertains to ion diffusion and transport in the electrolyte [25]. A short Warburg region on the plot can be explained by increased ion diffusion within the rGO electrodes due to the enhanced compatibility between the electrode and 0.5 M $[Bmim]^+Cl^-/H_2O$ electrolyte. The excellent capacitive behavior of 0.5 M $[Bmim^+Cl^-/H_2O$ electrolyte is also confirmed by a nearly vertical line at low frequencies [26]. From the extrapolation of the vertical portion of the Nyquist

plot to the real axis, the solution resistance was estimated to be 22, 13, 8, and 10 for pure, 0.1 M, 0.5 M, and 1 M $[Bmim]^+Cl^-/H_2O$ electrolyte respectively.

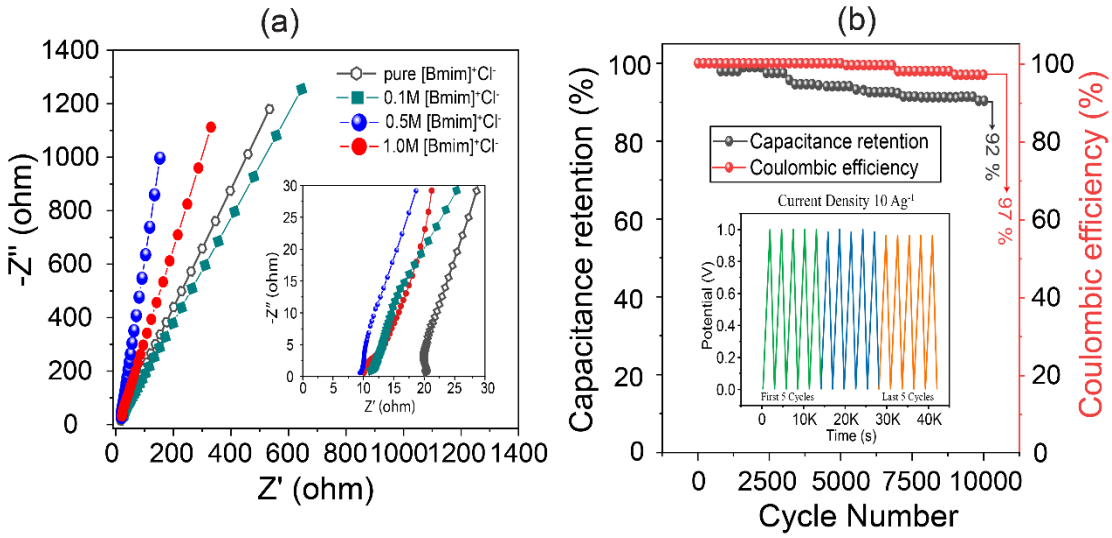

Figure 4.11. (a) Nyquist plot of rGO in pure and diluted $[Bmim]^+Cl^-$ electrolyte, (b) Cyclic performance of rGO in 0.5 M $[Bmim]^+Cl^-/H_2O$ electrolyte.

As previously mentioned, this is likely due to the lower electrical conductivity and higher viscosity of pure $[Bmim]^+Cl^-$ electrolytes. Nevertheless, the EIS furtherly proved that the negative impact from the lower ionic conductivity and high viscosity of the pure $[Bmim]^+Cl^-$ electrolyte may be offset by the water dilution in the operating voltage for achieving high energy and power density. Also, 0.5 M $[Bmim]^+Cl^-/H_2O$ electrolyte showed the highest conductivity, ion diffusion, as well as rate capability. Figure 4.11 (b) shows the variation of capacitance retention and coulombic efficiency with the increase in cycle number at a fixed current density of 10 A g^{-1}. The repeated cyclic performance of the rGO-based supercapacitor in the 0.5 M $[Bmim]^+Cl^-/H_2O$ electrolyte undergoes a slight degradation in coulombic efficiency and capacitance retention in 10000 charge-discharge cycles. The rGO retains ~97% of coulombic efficiency after 10000 cycles with ~92% of capacitance retention. The superior coulombic efficiency is related to the high effectiveness of the rGO-based supercapacitor for storing charges in 0.5 $[Bmim]^+Cl^-/H_2O$ electrolyte.

References

[1] Hidayah, N. M. S., Liu, W. W., Lai, C. W., Noriman, N. Z., Khe, C. S., Hashim, U., & Lee, H. C. (2017, October). Comparison on graphite, graphene oxide and reduced graphene oxide: Synthesis and characterization. In *AIP Conference Proceedings* (Vol. 1892, No. 1, p. 150002). AIP Publishing LLC.

[2] Magne, T. M., de Oliveira Vieira, T., Alencar, L. M. R., Junior, F. F. M., Gemini-Piperni, S., Carneiro, S. V., & Santos-Oliveira, R. (2021). Graphene and its derivatives: understanding the main chemical and medicinal chemistry roles for biomedical applications. *Journal of Nanostructure in Chemistry*, 1-35.

[3] Geng, J., Yin, Y., Liang, Q., Zhu, Z., & Luo, H. (2019). Polyethyleneimine cross-linked graphene oxide for removing hazardous hexavalent chromium: Adsorption performance and mechanism. *Chemical Engineering Journal*, *361*, 1497-1510.

[4] Soltani, T., & Lee, B. K. (2017). A benign ultrasonic route to reduced graphene oxide from pristine graphite. *Journal of Colloid and Interface Science*, *486*, 337-343.

[5] Zhang, W., Zou, X., & Zhao, J. (2015). Rapid production of a bulk of porous mesh reduced graphene oxide films using a naked flame. *Journal of Materials Chemistry C*, *3*(12), 2788-2791.

[6] Ebrahimi, S., Bordbar-Khiabani, A., Yarmand, B., & Asghari, M. A. (2019). Improving optoelectrical properties of photoactive anatase TiO2 coating using rGO incorporation during plasma electrolytic oxidation. *Ceramics International*, *45*(2), 1746-1754.

[7] Bhardwaj, J. S., Basumatary, P., Singh, A. K., & Agarwal, P. (2020, May). Comparative study of chemically and thermally reduced graphene oxide based on their specific surface area, structural and electrical properties. In *AIP Conference Proceedings* (Vol. 2220, No. 1, p. 020157). AIP Publishing LLC.

[8] Crosby, G. A., & Demas, J. N. (1971). Measurement of photoluminescence quantum yields. Review. *The Journal of Physical Chemistry*, *75*(8), 991-1024.

[9] Chu, J. H., Tong, L. B., Wen, M., Jiang, Z. H., Wang, K. S., & Zhang, H. J. (2019). Graphene oxide film as a protective barrier for Mg alloy: worse or better is dependent on a chemical reduction process. *Carbon*, *145*, 389-400.

[10] Tegou, E., Pseiropoulos, G., Filippidou, M. K., & Chatzandroulis, S. (2016). Low-temperature thermal reduction of graphene oxide films in ambient atmosphere: Infra-red spectroscopic studies and gas sensing applications. *Microelectronic Engineering*, *159*, 146-150.

[11] Tatlisu, A., Huang, Z., & Chen, R. (2018). High-Voltage and Low-Temperature Aqueous Supercapacitor Enabled by "Water-in-Imidazolium Chloride" Electrolytes. *ChemSusChem*, *11*(22), 3899-3904.

[12] Karaman, C., Karaman, O., Atar, N., & Yola, M. L. (2021). Sustainable electrode material for high-energy supercapacitor: biomass-derived graphene-like porous carbon with three-dimensional hierarchically ordered ion highways. *Physical Chemistry Chemical Physics*, *23*(22), 12807-12821.

[13] Lindberg, S. (2020). *Charge storage mechanisms and interactions of hybrid supercapacitor electrode materials with next-generation electrolytes* (Doctoral dissertation, Chalmers Tekniska Hogskola (Sweden)).

[14] Shao, H. (2020). *2D Ti3C2Tx MXenes for electrochemical energy storage* (Doctoral dissertation, Université Paul Sabatier-Toulouse III).

[15] Kim, T. Y., Lee, H. W., Stoller, M., Dreyer, D. R., Bielawski, C. W., Ruoff, R. S., & Suh, K. S. (2011). High-performance supercapacitors based on poly (ionic liquid)-modified graphene electrodes. *ACS nano*, *5*(1), 436-442.

[16] Chen, Q., Li, X., Zang, X., Cao, Y., He, Y., Li, P., & Zhu, H. (2014). Effect of different gel electrolytes on graphene-based solid-state supercapacitors. *RSC advances*, *4*(68), 36253-36256.

[17] Bayles, A. V., Valentine, C. S., Überrück, T., Danielsen, S. P., Han, S., Helgeson, M. E., & Squires, T. M. (2019). Anomalous solute diffusivity in ionic liquids: label-free visualization and physical origins. *Physical Review X*, *9*(1), 011048.

[18] Xie, J., Li, X., Lai, H., Zhao, Z., Li, J., Zhang, W., & Mai, W. (2019). A robust solid electrolyte interphase layer augments the ion storage capacity of bimetallic-sulfide-containing potassium-ion batteries. *Angewandte Chemie*, *131*(41), 14882-14889.

[19] Tatlisu, A., Huang, Z., & Chen, R. (2018). High-Voltage and Low-Temperature Aqueous Supercapacitor Enabled by "Water-in-Imidazolium Chloride" Electrolytes. ChemSusChem, 11(22), 3899-3904.

[20] Liang, T., Hou, R., Dou, Q., Zhang, H., & Yan, X. (2021). The Applications of Water-in-Salt Electrolytes in Electrochemical Energy Storage Devices. *Advanced Functional Materials*, *31*(3), 2006749.

[21] Anderson, J. L., Ding, R., Ellern, A., & Armstrong, D. W. (2005). Structure and properties of high stability geminal dicationic ionic liquids. *Journal of the American Chemical Society*, *127*(2), 593-604.

[22] Sun, Y., Ma, H., Zhang, X., Liu, B., Liu, L., Zhang, X., ... & Yan, X. (2021). Salty Ice Electrolyte with Superior Ionic Conductivity Towards Low-Temperature Aqueous Zinc Ion Hybrid Capacitors. *Advanced Functional Materials*, *31*(28), 2101277.

[23] Xiong, T., Lee, W. S. V., & Xue, J. (2018). K+-intercalated MnO2 electrode for high performance aqueous supercapacitor. *ACS Applied Energy Materials*, *1*(10), 5619-5626.

[24] Lvovich, V. F., & Smiechowski, M. F. (2006). Impedance characterization of industrial lubricants. *Electrochimica acta*, *51*(8-9), 1487-1496.

[25] An, F., Zhang, R., Wei, Z., & Li, P. (2019). Multi-stage constant-current charging protocol for a high-energy-density pouch cell based on a 622NCM/graphite system. *RSC advances*, *9*(37), 21498-21506.

[26] Afif, A., Rahman, S. M., Azad, A. T., Zaini, J., Islan, M. A., & Azad, A. K. (2019). Advanced materials and technologies for hybrid supercapacitors for energy storage–a review. *Journal of Energy Storage*, *25*, 100852.

Chapter-5

CONCLUSION

CONCLUSION

Choosing electrolytes that are stable over a large potential window is of great interest to improve the energy density of supercapacitors. This work chose a room temperature ionic liquid ($[Bmim]^+Cl^-$) with an electrochemical window approaching 2.4 V, and with a viscosity so high that it necessitates dilution with water. While past works provide evidence that dilution improves specific capacitance of devices at a certain rate, such measurements are heavily influenced by ionic and electronic transport due to both the measurement technique and porous nature of the electrodes. It has been shown here in a model system that dilution with water increases the intrinsic capacitance of $[Bmim]^+Cl^-$ on the rGO electrode, using CV, GCD, and EIS measurement. It is speculated that dilution accomplishes this by both increasing the concentration of dissociated ions and by screening the electrostatic interactions between free ions. As well as the surface science experiments of rGO and $[Bmim]^+Cl^-/H_2O$, could shed light on how exactly the introduction of solvent molecules serves to improve the double-layer capacitance. Additionally, a correlation has been made here between the minimum system resistance and maximum capacitance with dilution, indicating that parameters responsible for the behavior seen here may be tied to other bulk properties as well. However, the system resistance is not in itself a property of the electrolyte, and these data do not definitively correlate the intrinsic capacitance with any electrolyte properties. Future research will also involve looking at other bulk properties of the ionic $[Bmim]^+Cl^-/H_2O$ mixtures, such as ionic conductivity, viscosity, and dielectric constant, and considering whether any of these are correlated with the intrinsic capacitance trend seen here. Establishing these connections would be of great value in electrolyte optimization for supercapacitors and would help further the understanding of how co-solvents influence ionic liquid electrolytes. This work has also confirmed that dilution improves the specific capacitance of devices at a fixed current density. However, the device measurements have presented some limitations of this system than benefits. It proved difficult to operate the dilute ionic liquid electrolyte beyond 2.4 V. Part of the motivation for this work was to surpass what has been seen with less viscous ionic liquids, and that has not been accomplished. Further work is necessary to process devices with these electrolytes while still maintaining their purity and electrochemical window. It is important to make sure that the rGO sheets are present as single sheets when the ionic liquid is introduced. The tendency of this material to aggregate presents

a substantial research barrier and the processing technique used in this work must therefore be improved in order to increase the capacitance of devices. In other words, the dilution of a highly electrochemically stable ionic liquid presents more benefits than previously thought. However, additional work is necessary to pinpoint the physical nature of these benefits and to exploit these benefits in devices.